Long-term changes in light scattering in Chesapeake Bay inferred from Secchi depth, light attenuation, and remote sensing measurements

Charles L. Gallegos,[1] P. Jeremy Werdell,[2] and Charles R. McClain[2]

Received 22 March 2011; revised 2 August 2011; accepted 3 August 2011; published 27 October 2011.

[1] The relationship between the Secchi depth (Z_{SD}) and the diffuse attenuation coefficient for photosynthetically active radiation (K_d(PAR)), and in particular the product of the two, $Z_{SD} \cdot K_d$(PAR), is governed primarily by the ratio of light scattering to absorption. We analyzed measurements of Z_{SD} and K_d(PAR) at main stem stations in Chesapeake Bay and found that the $Z_{SD} \cdot K_d$(PAR) product has declined at rates varying from 0.020 to 0.033 yr^{-1} over the 17 to 25 years of measurement, implying that there has been a long-term increase in the scattering-to-absorption ratio. Remote sensing reflectance at the green wavelength most relevant to Z_{SD} and K_d(PAR) in these waters, R_{rs}(555), did not exhibit an increasing trend over the 10 years of available measurements. To reconcile the observations we constructed a bio-optical model to calculate Z_{SD}, K_d(PAR), $Z_{SD} \cdot K_d$(PAR), and R_{rs}(555) as a function of light attenuating substances and their mass-specific absorption and scattering coefficients. When simulations were based exclusively on changes in concentrations of light attenuating substances, a declining trend in $Z_{SD} \cdot K_d$ entailed an increasing trend in R_{rs}(555), contrary to observations. To simulate both decreasing $Z_{SD} \cdot K_d$(PAR) and stationary R_{rs}(555), it was necessary to allow for a declining trend in the ratio of backscattering to total scattering. Within our simulations, this was accomplished by increasing the relative proportion of organic detritus with high mass-specific scattering and low backscattering ratio. An alternative explanation not explicitly modeled is an increasing tendency for the particulate matter to occur in large aggregates. Data to discriminate between these alternatives are not available.

Citation: Gallegos, C. L., P. J. Werdell, and C. R. McClain (2011), Long-term changes in light scattering in Chesapeake Bay inferred from Secchi depth, light attenuation, and remote sensing measurements, *J. Geophys. Res.*, *116*, C00H08, doi:10.1029/2011JC007160.

1. Introduction

[2] The propagation of light underwater is a fundamental property of water that affects a large number of ecosystem processes as well as aesthetic judgments and suitability of water for certain designated human uses [*Davies-Colley et al.*, 2003]. Light penetration affects the balance of primary production between submersed aquatic vegetation (SAV) and phytoplankton [*Dennison et al.*, 1993], thereby affecting the flow of energy throughout the aquatic food web [*McClelland and Valiela*, 1998]. The ability to repetitively assess ocean color over global scales afforded by tandem developments in radiative transfer theory and instrumentation in support of remote sensing has added greatly to our understanding of global ocean productivity [*Falkowski et al.*, 1998].

[3] The instrumentation for measuring the apparent and inherent optical properties of water (AOPs and IOPs, respectively, in the sense of *Preisendorfer* [1961]; see notation section for symbols, abbreviations and acronyms) has advanced rapidly in recent years. It is now possible to make the measurements of IOPs in situ and boundary conditions sufficient to obtain closure between measured and modeled AOPs in optically complex waters [*Chang et al.*, 2003; *Tzortziou et al.*, 2006; *Gallegos et al.*, 2008]. However, that instrumentation is relatively new and consequently, long-term measurements of IOPs from any one location are not available. Much less sophisticated techniques have been in use much longer. Measurements of Secchi depth date back to the 19th century [*Boyce et al.*, 2010], and long-term records (>30 years) on individual water bodies have been useful in documenting declines in water clarity due to development in the watershed [*Jassby et al.*, 2003] and regime shifts due to different combinations of top-down (zooplankton) and bottom-up (nutrient reduction) effects [*Effler et al.*, 2008].

[4] Submersible sensors for measuring the photon flux density of photosynthetically active radiation (PAR, 400–700 nm) have been in wide use since the 1970s. A long-

[1]Smithsonian Environmental Research Center, Edgewater, Maryland, USA.
[2]Ocean Ecology Branch, NASA Goddard Space Flight Center, Greenbelt, Maryland, USA.

0148-0227/11/2011JC007160

standing motive for the development and use of submersible PAR sensors has been to measure the diffuse attenuation for downwelling PAR (i.e., K_d(PAR)) for the calculation of the depth distribution of phytoplankton photosynthesis from photosynthesis-irradiance curves [*Ryther and Yentsch*, 1957; *Platt et al.*, 1990]. In cases where PAR sensors have not been available, there has been a desire to estimate K_d(PAR) from Secchi depth measurements [*Poole and Atkins*, 1929]. The relationship of Secchi depth to K_d(PAR) has usually been studied for the purpose of estimating the latter from the former [e.g., *Idso and Gilbert*, 1974; *Koenings and Edmundson*, 1991], focusing on the product of the two, $Z_{SD} \cdot K_d$(PAR) (Z_{SD} = Secchi depth). Because of its dependence on the relative strength of scattering and absorption (see below), the $Z_{SD} \cdot K_d$(PAR) product is an indicator of turbid particulate and color loading [*Koenings and Edmundson*, 1991]. It is equivalent to the optical depth of the Secchi depth, and is important because it determines the conversion between Secchi depth and photic depth (conventionally, the depth of penetration of 1% of surface irradiance). *Poole and Atkins* [1929] determined the $Z_{SD} \cdot K_d$(PAR) product to average 1.7 (range 1.32 to 2.18, dimensionless) for waters off Plymouth, UK, a value supported by *Idso and Gilbert* [1974], who extended the analysis to turbid waters with Secchi depth as low as 0.09 m. *Koenings and Edmundson* [1991] found distinctly different median values of the $Z_{SD} \cdot K_d$(PAR) product in clear lakes (median $Z_{SD} \cdot K_d$(PAR) = 1.86), humic-stained lakes (median 2.7), and turbid water bodies (median 0.93). For this range, the photic depth can be as low as a factor of 1.7 times Z_{SD} or as great as 4.95 times Z_{SD}. Therefore, when estimating the photic depth from Z_{SD}, uncertainty in the value of $Z_{SD} \cdot K_d$(PAR) for a water body can translate into potential errors in estimates of primary productivity if the extent of the photic zone is misrepresented in sampling the water body and integration of productivity versus depth curves.

[5] Theoretical analyses of the $Z_{SD} \cdot K_d$(PAR) product by *Effler* [1985] and *Davies-Colley and Vant* [1988] drew upon analyses of Secchi disk transparency by *Tyler* [1968] and *Preisendorfer* [1986], and the analyses of diffuse attenuation coefficient by *Kirk* [1981, 1984]. These authors demonstrated that the $Z_{SD} \cdot K_d$(PAR) product was dependent to a high degree on the ratio of scattering to absorption [*Effler*, 1985; *Davies-Colley and Vant*, 1988], and emphasized the diagnostic utility of the $Z_{SD} \cdot K_d$(PAR) product in assessing the scattering-to-absorption ratio of a water body.

[6] An interest in calculating phytoplankton productivity from chlorophyll and irradiance at synoptic to global scales has similarly motivated many developments in satellite remote sensing [*Platt and Herman*, 1983; *Platt and Sathyendranath*, 1988]. The remote sensing reflectance, R_{rs}, received by a satellite after correction for atmospheric distortion is approximated by [*Gordon et al.*, 1975]

$$R_{rs} \propto \frac{b_b}{a + b_b} = \frac{\tilde{b}_b b/a}{a + \tilde{b}_b b/a} \tag{1}$$

where a = absorption coefficient, b = scattering coefficient, b_b = backscattering coefficient, and $\tilde{b}_b$ = ratio of backscattering to total scattering. The spectral properties of a and b_b carry information about the particulate and dissolved content of the water. Therefore R_{rs}, like $Z_{SD} \cdot K_d$(PAR), depends to a high degree on the scattering-to-absorption ratio of the water body, b/a, but also on $\tilde{b}_b$. The dependence of $Z_{SD} \cdot K_d$(PAR) on $\tilde{b}_b$ has not been investigated.

[7] Much has been learned both theoretically [*Stramski et al.*, 2001; *Babin et al.*, 2003a; *Woźniak and Stramski*, 2004] and empirically [*Babin et al.*, 2003b; *Peng and Effler*, 2007; *Bowers et al.*, 2009] about the scattering properties of various components of particulate matter since these analyses of $Z_{SD} \cdot K_d$(PAR) and R_{rs}, permitting some generalizations to be reached. The mass-specific absorption and scattering coefficients and backscattering ratio of particulates are functions of the size, shape, and composition of particles [*Stramski et al.*, 2001; *Babin et al.*, 2003a; *Clavano et al.*, 2007]. In general, other things being equal, smaller particles absorb and scatter light more strongly on a mass-specific basis than larger particles; and particles with higher index of refraction (i.e., minerals compared with organics) scatter light more strongly than those with lower indices of refraction. However, the higher specific gravity of mineral particles means that, when normalized to particle mass, the mass-specific scattering and absorption coefficients of mineral particles tend to be lower than those of organic particles [*Babin et al.*, 2003a]. The backscattering ratios of minerogenic particles are much higher than those of organic particles (approximately thirtyfold) [*Stramski et al.*, 2004]. Based on these different properties, changes in the relative composition of the particulate pool of a water body may lead to contrasting changes in R_{rs} and the $Z_{SD} \cdot K_d$(PAR) product that have diagnostic value.

[8] Here we briefly review these previous theoretical treatments of the $Z_{SD} \cdot K_d$(PAR) product and introduce a modification to incorporate recent advances in understanding of the variability in the particulate backscattering-to-scattering ratio. We demonstrate that, unlike R_{rs}, the dependence of $Z_{SD} \cdot K_d$(PAR) on $\tilde{b}_b$ is weak, so that simultaneous observations of long-term records of $Z_{SD} \cdot K_d$(PAR) and R_{rs} offer potential to track changes in the particulate backscattering-to-scattering ratio. We then examine long-term changes in the $Z_{SD} \cdot K_d$(PAR) product and remote sensing reflectance in Chesapeake Bay. To derive possible explanations for observed trends we construct a bio-optical model of diffuse attenuation coefficient, Secchi depth, and remote sensing reflectance to examine the sensitivity of the $Z_{SD} \cdot K_d$(PAR) product to concentrations, composition, and mass-specific optical properties of the light attenuating substances (LAS).

2. Theory

[9] Previous derivations of the $Z_{SD} \cdot K_d$(PAR) product multiplied *Preisendorfer*'s [1986] expression for Z_{SD} and *Kirk*'s [1984] equation for K_d to arrive at the expression [*Effler*, 1985; *Davies-Colley and Vant*, 1988]

$$Z_{SD} \cdot K_d(\mathrm{PAR}) = \frac{\Gamma\left(1 + G(\mu_0)\frac{b}{a}\right)^{1/2}}{\left(1 + G(\mu_0)\frac{b}{a}\right)^{1/2} + \mu_0\left(1 + \frac{b}{a}\right)} \tag{2}$$

where Γ is a coupling constant with additional dependencies to be discussed below, μ_0 is the cosine of the in-water solar zenith angle, and $G(\mu_0)$ is a linear function that scales the

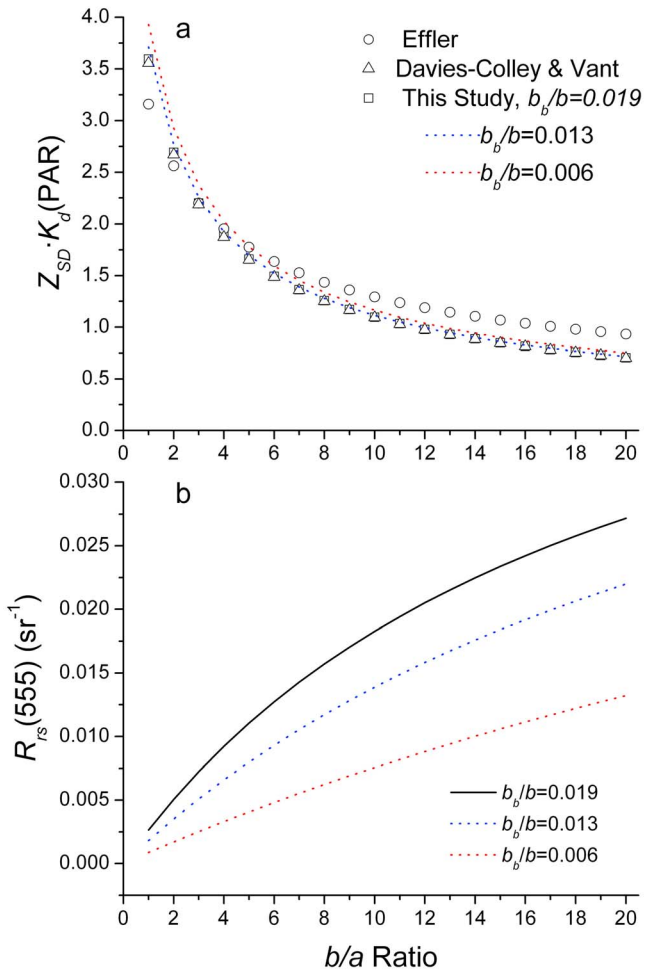

Figure 1. (a) Relationship of the product of Secchi depth, Z_{SD}, and diffuse attenuation coefficient for PAR, K_d(PAR), to the scattering-to-absorption ratio, as calculated by *Effler* [1985] (circles), *Davies-Colley and Vant* [1988] (triangles), and this study (squares), backscatter ratio = 0.019. *Effler* [1985] treated Γ (equation (8)) as constant, whereas *Davies-Colley and Vant* [1988] calculated Γ as a function of reflectance (equation (4)) for a fixed backscattering ratio of 0.019. Dotted lines show range of variation in $Z_{SD} \cdot K_d$(PAR) for backscattering ratio from (blue) 0.013 to (red) 0.006. (b) Relationship of remote sensing reflectance at 555 nm to the scattering-to-absorption ratio at three values of the backscatter ratio as in Figure 1a, for a constant absorption coefficient at 555 nm of 0.36 m^{-1}.

interactive effect of absorption and scattering on diffuse attenuation.

[10] Equation (2) is strongly governed by the scattering-to-absorption ratio, b/a. Effler treated Γ as a constant [*Effler*, 1985] or a random variable [*Effler et al.*, 2005], whereas *Davies-Colley and Vant* [1988] modeled Γ as an expanded function of reflectance, R, based on *Tyler* [1968],

$$\Gamma = \ln\left(\frac{C_0}{C_T}\right) = \ln\left(\frac{R_{disk} - R}{C_T R}\right) \tag{3}$$

where C_0 is the apparent contrast between the Secchi disk and the surrounding medium, C_T is the threshold contrast, and R_{disk} is the reflectivity of the white paint on the Secchi disk. Noting that reflectance of the medium and the scattering-to-absorption ratio are interrelated, *Davies-Colley and Vant* [1988] used *Kirk* [1984] to interpolate b/a from R and μ_0 such that equation (2) could be evaluated in terms or R or b/a interchangeably.

[11] These earlier treatments of the $Z_{SD} \cdot K_d$(PAR) product were based on *Kirk*'s [1984] Monte Carlo radiative transfer model. This model used a single scattering phase function based on turbid San Diego Harbor [*Petzold*, 1972], which has a backscattering-to-scattering ratio, $\tilde{b}_b$ = 0.019 [*Kirk*, 1994]. The scattering phase function affects $G(\mu_0)$ and, to a lesser degree, the relationship between R and b/a [*Kirk*, 1994]. Subsequent to those studies, much more information has become available on the regional variability of $\tilde{b}_b$ [*Boss et al.*, 2004; *Tzortziou et al.*, 2006; *Loisel et al.*, 2007] and its dependence on the water composition [*Stramski et al.*, 2001]. This improved availability of backscattering information allows us to incorporate the dependence of R in equation (3) on b/a from remote sensing relationships [*Morel and Gentili*, 1993],

$$R = f' \frac{b_b}{a} = f' \tilde{b} \frac{b}{a} \tag{4}$$

where the bidirectional coefficient, f', is a function of the solar zenith angle and the single scattering albedo, b/c. Here we chose this expression for R for its explicit dependence on b/a, the common term in equation (2). In constructing a bio-optical model of remote sensing reflectance (see below) we used the form more appropriate for highly scattering coastal waters proportional to $b_b/(a + b_b)$. Substitution of equation (4) into (3) and (2) results in prediction of monotonically decreasing $Z_{SD} \cdot K_d$(PAR) product as a function of b/a (Figure 1a). The calculations with $\tilde{b}_b$ = 0.019 had a greater range than that predicted using constant Γ [*Effler*, 1985], but differed little from that predicted using *Kirk*'s [1984] expression for f' [*Davies-Colley and Vant*, 1988].

[12] The dependence of $Z_{SD} \cdot K_d$(PAR) on $\tilde{b}_b$ is relatively weak (Figure 1a) varying less than 10 percent as $\tilde{b}_b$ is varied threefold with values chosen to approximate phytoplankton ($\tilde{b}_{bp}$ = 0.006), the average for mesohaline Chesapeake Bay ($\tilde{b}_{bp}$ = 0.013) [*Tzortziou et al.*, 2006] and the "Petzold average" ($\tilde{b}_{bp}$ = 0.019) [*Petzold*, 1972]. In marked contrast, remote sensing reflectance calculated by equation (1) using a proportionality constant of 0.0529 (see below) and constant a(555) (0.36 m^{-1}, typical scale for mid Chesapeake Bay) is highly dependent on both b/a and on $\tilde{b}_b$ (Figure 1b). The combination of strong sensitivity to $\tilde{b}_b$ of R_{rs} and weak sensitivity of $Z_{SD} \cdot K_d$(PAR) means that simultaneous observations of R_{rs} and $Z_{SD} \cdot K_d$(PAR) have the potential to provide information about possible changes in $\tilde{b}_b$. For example, changes in the concentration or composition of particulate matter that resulted in an increase in b/a with constant $\tilde{b}_b$ would be expected to increase R_{rs} along a curve similar to those in Figure 1b, whereas a constant or declining R_{rs} would signal a decrease in $\tilde{b}_b$.

3. Data Sources and Methods

3.1. In Situ Measurements

[13] Simultaneous measurements of K_d(PAR) and Z_{SD} for the main stem of Chesapeake Bay were made by the

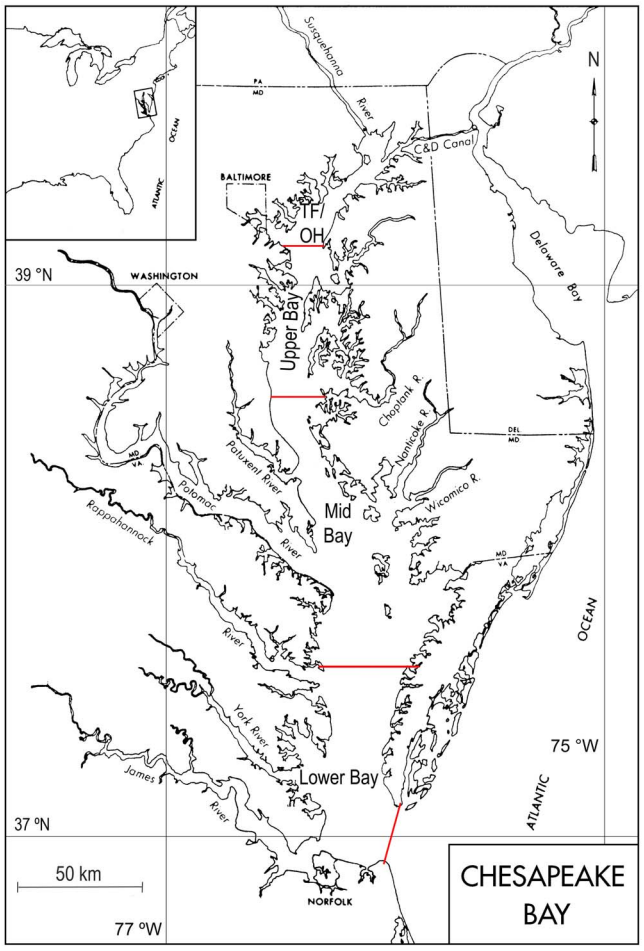

Figure 2. Map of Chesapeake Bay showing segmentation scheme (red lines) for aggregating measurements of Z_{SD}, K_d(PAR), and water quality. Inset shows location of Chesapeake Bay in mid-Atlantic region.

Chesapeake Bay Program (CBP) Water Quality Monitoring Program from 1987 to 2009. Data were downloaded from the Chesapeake Information Management System (CIMS) database, http://www.chesapeakebay.net/data_waterquality.aspx. Ancillary measurements downloaded with the K_d(PAR) and Z_{SD} data include total suspended solids (*TSS*) and chlorophyll *a* (*CHLA*) in near-surface samples, generally from 0.5 m in Maryland and 1.0 m in Virginia. CDOM measurements were downloaded for a limited collection period from 2005 to 2006 (April through October). We focus the analysis on main stem stations. Measurements were averaged by segments as defined by *Magnuson et al.* [2004]: Lower Bay, south of 37.6°N; mid-Bay, 37.6 to 38.6°N; upper Bay, 38.6 to 39.2°N (Figure 2). Additionally, we examined in situ measurements from tidal fresh and oligohaline (TF/OH) main stem stations north of 39.2°N for which there are no reliable corresponding remote sensing measurements due to adjacency effects (stray light from land) and the high turbidity and CDOM concentrations in this region. Data were analyzed by general linear model (GLM), treating year as a continuous variable to estimate the slopes of long-term trends, and month as a categorical variable to allow for seasonality.

3.2. Remote Sensing Measurements

[14] Time series of SeaWiFS and MODIS-Aqua Level-2 data products for Chesapeake Bay were acquired from the NASA Ocean Biology Processing Group (http://oceancolor.gsfc.nasa.gov). The time series spanned late 1997 through 2008 and mid-2002 through 2008, at approximately ~1.1 km^2 spatial resolution. Satellite data processing and quality assurance for the time series followed *Werdell et al.* [2009] using reprocessing configurations R2010.0 (September 2010) and R2009.1 (April 2010) for SeaWiFS and MODIS-Aqua, respectively. We calculated monthly geometric means of all available (unmasked) data for each Chesapeake Bay subregion of interest. After application of quality assurance metrics, the monthly means included data from approximately 10 days per month.

4. Bio-optical Model

4.1. Apparent Optical Properties

[15] As an aid for interpreting changes in $Z_{SD} \cdot K_d$(PAR) we constructed a bio-optical model that computes the quantities needed to form $Z_{SD} \cdot K_d$(PAR) and R_{rs} in terms of suspended and dissolved constituents. The model computes absorption, scattering, and backscattering spectra for use in the equation for spectral diffuse attenuation coefficient of *Lee et al.* [2005] and *Preisendorfer*'s [1986] equation for Secchi depth. We considered 2 scenarios of differing complexity: in scenario 1 we allowed concentrations of LAS and mass-specific IOPs to vary in a standard Case 2 bio-optical model; in scenario 2 we disaggregated the total particulate matter into subpopulations having mass-specific optical properties drawn from the literature.

[16] For spectral diffuse attenuation coefficients, we use the model of *Lee et al.* [2005] because it is expressed in terms of backscattering rather than total scattering [e.g., *Kirk*, 1984], and can, therefore, predict the effects of changes in the relative proportions of particulate components having different backscattering ratios. The model of *Lee et al.* [2005] is given by

$$K_d(\lambda) = (1 + 0.005\theta_0)a(\lambda) + 4.18\{1 - 0.52\exp[-10.8a(\lambda)]\}b_b(\lambda) \quad (5)$$

where θ_0 is the solar incidence angle in degrees, and $a(\lambda)$ and $b_b(\lambda)$ spectra are simulated from concentrations of LAS (see below). To correspond with measurements we calculated K_d(PAR) from spectral $K_d(\lambda)$ by propagating the spectrum of surface incident irradiance to a reference depth, z, by the Beer-Lambert law,

$$E_d(z, \lambda) = E_0(\lambda)\exp[-K_d(\lambda)z] \quad (6)$$

where $E_d(z, \lambda)$ is the downwelling spectral irradiance at depth z and $E_0(\lambda)$ is the surface incident downwelling irradiance converted to quantum units. We then calculated PAR at the surface (0) and depth z by numerical integration, and

$$K_d(PAR) = -\frac{1}{z}\ln\left(\frac{PAR_z}{PAR_0}\right). \quad (7)$$

For standardization of calculations, we used z = 4 m and calculated $E_0(\lambda)$ using the RADTRAN routine in the radia-

tive transfer program *Hydrolight* [*Mobley*, 1994] for 1 June, 1100 local standard time at a central Bay location of 38.5°N, 76.3°W.

[17] We calculated Z_{SD} according to the equation of *Preisendorfer* [1986]

$$Z_{SD} = \frac{\Gamma}{c + K_d} \tag{8}$$

with Γ calculated by equation (3) with the beam attenuation coefficient c (= a + b) and K_d evaluated at 555 nm, close to the most penetrating wavelength in middle and lower Chesapeake Bay, and at the maximum sensitivity of the light-adapted human eye [*Davies-Colley et al.*, 2003]. We assumed a contrast threshold, C_t = 0.066, disk reflectivity, R_{disk} = 0.82 [*Davies-Colley and Vant*, 1988], and calculated in situ reflectance by equation (4) with f' evaluated according to *Morel and Gentili* [1993] as cited by *Hirata and Højerslev* [2008].

[18] We calculated above-water, nadir-viewing remote sensing reflectance at 555 nm, R_{rs}(555), using the total absorption and backscattering coefficients calculated as given below,

$$R_{rs}(555) = 0.0529 \frac{b_b(555)}{a(555) + b_b(555)} \tag{9}$$

where the proportionality constant, 0.0529 sr^{-1}, was interpolated from the measurements in Chesapeake Bay at 532 and 650 nm by *Tzortziou et al.* [2006] and is close to theoretical expectations for waters with optical signatures dominated by phytoplankton [*Morel et al.*, 2002]. A scenario to examine the sensitivity of our main conclusions to the assumption of constant proportionality coefficient in equation (9) is presented in the auxiliary material.[1]

4.2. Inherent Optical Properties of Light Attenuating Substances

[19] We partitioned absorption into components due to water, dissolved substances, and particulates,

$$a(\lambda) = a_w(\lambda) + a_g(\lambda) + a_p(\lambda) \tag{10}$$

where a_w, a_g, and a_p are the absorption due to water, CDOM, and particulate matter, respectively. We used the pure water absorption spectrum of *Pope and Fry* [1997]. We expressed absorption by particulate matter as the sum of that due to phytoplankton pigments, $a_\phi(\lambda)$, and that due to nonalgal particulates (NAP), $a_{NAP}(\lambda)$. The NAP pool is a heterogeneous mixture of minerals, detritus, and heterotrophic organisms, for which we attempt a further decomposition below.

[20] We partitioned backscattering into contributions by water and particulate components,

$$b_b(\lambda) = b_{bw}(\lambda) + b_{b\phi}(\lambda) + b_{bNAP}(\lambda) \tag{11}$$

where the subscripted b denotes the backward direction, and as before, the subscripts w, ϕ, and NAP stand for water, phytoplankton, and nonalgal particulates, respectively (CDOM is considered nonscattering [*Mobley and Stramski*, 1997]). Backscattering by particulate components is frequently characterized by the backscattering ratio, $\tilde{b}_{bp}$, i.e., the fraction of particulate scattering that is in the backward direction [*Stramski et al.*, 2001; *Snyder et al.*, 2008]. The backscattering coefficient may then be represented in terms of the partial backscattering ratios and total scattering by pure water and particulate components,

$$b_b(\lambda) = \tilde{b}_{bw} b_w(\lambda) + \tilde{b}_{b\phi} b_\phi(\lambda) + \tilde{b}_{bp} b_{NAP}(\lambda) \tag{12}$$

where the b_x and $\tilde{b}_{bx}$ are the total scattering coefficients and backscattering ratios, respectively, for component x, and the subscripts are as previously given. Molecular scattering is taken to be isotropic, i.e., $\tilde{b}_{bw}$ = 0.5 [*Mobley*, 1994]. The backscattering ratios of the particulate components are much smaller, and will be discussed in sections 4.2.2 and 4.2.3. Even so, in coastal waters, backscattering by particulate matter greatly exceeds that by pure water because total particulate scattering is so much greater than molecular scattering by water. The spectral variability of the backscattering ratio is difficult to generalize [*Snyder et al.*, 2008]. For this analysis, we assumed constant $\tilde{b}_{bp}$ across visible wavelengths.

4.2.1. CDOM

[21] We represent the absorption by CDOM as a negative exponential [*Bricaud et al.*, 1981] scaled by its value at 440 nm, i.e., a_g(440),

$$a_g(\lambda) = a_g(440) \exp\left[-s_g(\lambda - 440)\right] \tag{13}$$

where s_g is the spectral slope of absorption by CDOM. Bay-wide measurements of a_g(440) and s_g made from 2005 to 2006 are available to guide simulation of variability in CDOM absorption (Table 1).

4.2.2. Phytoplankton

[22] To model light absorption by phytoplankton, we represented the average spectral shape by the spectrum normalized to the value at the absorption peak at 675 nm, i.e.,

$$\phi(\lambda) = \frac{a_\phi(\lambda)}{a_\phi(675)} \tag{14a}$$

where $\phi(\lambda)$ is the normalized absorption by phytoplankton. We used a normalized absorption spectrum measured on samples from midchannel upper Bay stations occupied by *Tzortziou et al.* [2006] in May, June, and November 2002. Samples collected at these times are expected to be dominated by diatoms [*Magnuson et al.*, 2004]. To scale the overall absorption by phytoplankton we determine the chlorophyll-specific absorption coefficient at 675 nm, a_ϕ^*(675), and calculate a_ϕ(675) from chlorophyll concentration (*CHLA*),

$$a_\phi(675) = a_\phi^*(675)[CHLA]. \tag{14b}$$

[23] In scenario 1 a_ϕ^*(675) was held constant at 0.025 m^2 (mg Chla)$^{-1}$ [*Magnuson et al.*, 2004], and in scenarios 2 it was allowed to vary between 0.013 and 0.04 m^2 (mg Chla)$^{-1}$ [*Bricaud et al.*, 1995].

[1] Auxiliary materials are available in the HTML. doi:10.1029/2011JC007160.

Table 1. Average, Minimum, Maximum, and Number of Measurements of CDOM Absorption Coefficient at 440 nm, $a_g(440)$ (m^{-1}), and Spectral Slope, s_g (nm^{-1}), in Main Stem Segments of Chesapeake Bay Measured From July 2005 to June 2006 (April Through August)[a]

	$a_g(440)$ (m^{-1})			s_g (nm^{-1})			
Segment	Average	Minimum	Maximum	Average	Minimum	Maximum	n
TFOH	0.551	0.292	1.334	0.0169	0.0158	0.0189	49
Upper	0.427	0.282	1.004	0.0173	0.0150	0.0221	108
Mid	0.373	0.249	1.293	0.0174	0.0143	0.0201	140
Lower	0.293	0.123	0.650	0.0174	0.0140	0.0207	144

[a]Data were downloaded from the Chesapeake Information Management System (CIMS) database (http://www.chesapeakebay.net/data_waterquality.aspx). Segment boundaries are given in the text and in Figure 1; n, number of measurements.

[24] Scattering by phytoplankton was taken to be proportional to the organic carbon content of the phytoplankton converted to dry weight according to

$$SPM_\phi = \frac{2.6[CHLA]\theta}{1000} \tag{15}$$

where SPM_ϕ (g m^{-3}) is the dry weight, θ is the phytoplankton C:CHLA ratio (g g^{-1}), division by 1000 converts mg to g, and 2.6 (g g^{-1}) is an approximate ratio of dry weight to particulate organic carbon [*Babin et al.*, 2003a]. Scattering is given by

$$b_p^\phi(\lambda) = b_\phi^*(555)SPM_\phi\left(\frac{555}{\lambda}\right)^{\eta_\phi} \tag{16}$$

where b_p^ϕ is the particulate scattering by phytoplankton, b_ϕ*(555) is the mass-specific scattering coefficient of phytoplankton on a dry weight basis at 555 nm, and η_ϕ is the exponent of the power law describing particulate scattering. We treat phytoplankton as large organic particles, hence take $\eta_\phi = 0$ (scattering spectrally invariant) and set b_ϕ*(555) = 0.6 m^2 g^{-1} in both scenarios [*Babin et al.*, 2003a, Figure 6] (Junge slope = 3.6, see below). According to the analysis by *Stramski et al.* [2001], $\tilde{b}_{b\phi}$ is of order 10^{-3}, with most of their simulated curves for a wide range of phytoplankton species clustering around 0.003 [*Stramski et al.*, 2001, Figure 4]. An alternative, chlorophyll-dependent formulation of scattering and backscattering by phytoplankton based on relationships observed in Case 1 waters [*Huot et al.*, 2008] is presented in the auxiliary material.

4.2.3. Nonalgal Particulates

[25] The concentration of nonalgal particulates (NAP) is quantified by the measurement of total suspended solids (TSS), although it is important to recognize that the dry weight of phytoplankton, SPM_ϕ, contributes to TSS. The diverse components that comprise NAP (e.g., organic detritus, bacteria, microzooplankton, mineral particulates) have mass-specific optical properties which differ from one another [*Bowers and Binding*, 2006; *Morel and Ahn*, 1990, 1991; *Stramski et al.*, 2001]. The varying (and largely unknown) composition of NAP means that there potentially is large variability in the relationship between IOPs and TSS.

[26] The specific absorption spectrum of NAP can be represented [*Bowers and Binding*, 2006]

$$a_x^*(\lambda) = c_1^x + c_2^x \exp[-s_x(\lambda - 440)] \tag{17}$$

where a_x*(λ) is the specific absorption spectrum, x allows different mass-specific IOPs for the different NAP components, c_1 allows for the possibility of some absorption at long wavelengths, c_2 scales the absorption at the reference wavelength (440 nm), and s_x governs the rate of exponential decline with wavelength. In scenario 1 we varied the values of c_1 and c_2 to simulate unspecified changes in the relative composition of the NAP.

[27] In scenario 2 we considered the NAP pool to be mixtures of four types of particles representing "small" and "large" optical end-members of organic and mineral particles. We represented NAP absorption by equation (17) with coefficients varying among the four components (Table 2). We represented scattering and backscattering for each component similar to equation (16), with separate mass-specific scaling coefficients at 555 nm, b_x*(555), spectral exponents η_x, and wavelength-independent backscattering ratios, $\tilde{b}_{bx}$, for each component [*Stramski et al.*, 2004]. Coefficients assigned to each particulate subcomponent are summarized in Table 2 and discussed below.

[28] Absorption by NAP has been investigated theoretically by *Stramski et al.* [2001] and synthesized from field studies by *Bowers and Binding* [2006]. The existence of particulate absorption at long wavelengths (c_1) is controversial and unsettled, with some authors claiming to have measured it [*Tassan and Ferrari*, 2003; *Bowers and Binding*, 2006; *Tzortziou et al.*, 2006], and others claiming that careful elimination of scattering in the measurement apparatus eliminates it [*Babin and Stramski*, 2002]. Here we assigned a nonzero value to one component, small minerals, because the analyses by Bowers and Binding emphasized mineral-dominated waters, and some long-wavelength absorption was necessary to achieve radiative transfer closure in Chesapeake Bay [*Tzortziou et al.*, 2006].

[29] Values assigned to c_2 in Table 2 reflect the observation that organic particulates tend to be more colored (light absorbing) than mineral particulates, with our values for small detritus modeled after the Baltic [*Woźniak and*

Table 2. Coefficients Used in Equations Governing the Absorption, Scattering, and Backscattering by Different Components of the Nonalgal Particulate Pool

Parameter	Small Organic Detritus	Large Organic Detritus	Small Minerals	Large Minerals
c_1 (m^2 g^{-1})	0	0	0.016	0
c_2 (m^2 g^{-1})	0.08	0.044	0.054	0.024
s_x (nm^{-1})	0.013	0.0124	0.012	0.011
b_x*(555) (m^2 g^{-1})	1.15	0.6	0.80	0.24
η (dimensionless)	0.5	0	0.97	0.22
$\tilde{b}_{bx}$ (dimensionless)	0.005	0.003	0.04	0.019

Table 3. Probability Distributions and Associated Parameters (P1, P2) Used for Simulating Concentrations of Components in Monte Carlo Simulation With the Bio-optical Model[a]

Component	Distribution (P1, P2)	Scenario
CDOM (m^{-1})	Lognormal (0.39, 0.072)	1, 2
CHLA (mg m^{-3})	Lognormal (15, 10)	1, 2
TSS (g m^{-3})	Lognormal (8.5, 8)	1
a_ϕ*(675) (m^2 mg^{-1})	Uniform (0.013, 0.04)	1, 2
c_1 (m^2 g^{-1})	Uniform (0, 0.05)	1
c_2 (m^2 g^{-1})	Uniform (0.02, 0.16)	1
b_p*(555) (m^2 g^{-1})	Uniform (0.2, 1.4)	1
$\tilde{b}_{bp}$	Uniform (0.007, 0.040)	1
Small organic detritus (g m^{-3})	Uniform (0, 10)	2
Small minerals (g m^{-3})	Uniform (0, 10)	2
Large minerals (g m^{-3})	Uniform (0, 2)	2
θ (mg C [mg CHLA]$^{-1}$)	Uniform (30, 100)	2
SPM_ϕ (g m^{-3})	Lognormal (2.58, 2.31)[b]	2

[a]Parameters of uniform distribution are (minimum, maximum); parameters of lognormal distribution are (mean, standard deviation). Scenario numbers refer to scenarios in which water quality and mass-specific IOPs were varied (scenario 1) and in which water quality, phytoplankton chlorophyll-specific absorption, and components of particulate submodel were varied (scenario 2).

[b]Determined empirically as the result of equation (15) and underlying assumptions for CHLA and θ.

Dera, 2007], large organics based on Case 1 (i.e., optical properties governed by phytoplankton and their byproducts) waters of the Atlantic [*Babin et al.*, 2003b], small minerals from the Irish Sea [*Bowers and Binding*, 2006], and large minerals after the tidally energetic waters of Menai Strait [*Bowers and Binding*, 2006]. Spectral slopes, s_x, are remarkably similar among particle types, with slightly higher values for more colored organic particles [*Babin et al.*, 2003a, 2003b].

[30] Based on the theoretical analysis of *Babin et al.* [2003a], we assigned the highest mass-specific scattering coefficient to small organic detritus, and the lowest to large minerals. In theoretical studies of light scattering and absorption by particles several authors have fit the size distribution of particles to a Junge-type function given by [*Boss et al.*, 2001; *Twardowski et al.*, 2001; *Babin et al.*, 2003a]

$$N(D) \propto D^{-j} \tag{18}$$

where D is the particle diameter and j is the slope of the distribution; the higher the value of j, the greater the domination of the distribution by smaller particles. Our values for b_p*(555) and η in Table 2 reflect values of $j = 4.2$ for small organic detritus, $j = 3.4$ for large organic detritus, $j = 4$ for small minerals, and $j = 3.4$ large minerals from *Babin et al.* [2003a, Figure 6 and Table 6]. Our reference to the Junge size distribution makes no assumption about the accuracy of this function for natural particle assemblages. We simply use the slope j as a single-parameter indicator of size for characterizing the bulk IOPs of the end-member particle types. Our specific scattering coefficients for the mineral end-members are remarkably similar to the highest and lowest curves in the mineral-dominated field samples of *Woźniak et al.* [2010, Figure 7a].

[31] We based our selection of backscattering ratios on the analysis of *Stramski et al.* [2001] and field surveys of *Loisel et al.* [2007] and *Snyder et al.* [2008]. Scattering by organic particles is strongly in the forward direction, hence the smallest value of $\tilde{b}_{bp}$ was assigned to large organic detritus, followed by small organic detritus (Table 2). Mineral particles, having indices of refraction higher than those of organic particles, scatter a greater fraction of light in the backward direction, and this is reflected in the values of $\tilde{b}_{bp}$ for small and large minerals in Table 2. The highest value of $\tilde{b}_{bp}$ in Table 2, 0.04, is the same as used by *Stramski et al.* [2001], so that the simulated bulk values should span most of the range of values observed in field studies (0.0024 to 0.06) [*Loisel et al.*, 2007; *Snyder et al.*, 2008].

[32] This partitioning of the NAP allows us to calculate some commonly measured parameters: *TSS* is the sum of all 4 components; particulate organic matter (*POM*) is the sum of small organic detritus + SPM_ϕ; and the fractional organic content is given by $f_{org} = POM/TSS$. Additionally, in scenario 2 the mass-specific absorption and backscattering coefficients for *TSS* become computed rather than assumed values as in scenario 1.

4.3. Simulation Approach

[33] We took a Monte Carlo modeling approach whereby we assigned random numbers to the concentrations of CDOM, CHLA and TSS and the mass-specific IOPs (scenario 1). We then varied concentrations of the component populations of the nonalgal particulates and θ (scenario 2). In each scenario we simulated 60,000 realizations of Z_{SD}, K_d(PAR), $Z_{SD} \cdot K_d$(PAR), and R_{rs}(555), then, based on observations reported in section 5, sorted the data by simulated $Z_{SD} \cdot K_d$(PAR) in descending order as a surrogate for time. We used ranges of observed variables to select simulations appropriate for different segments of the Bay, then compared the patterns of simulated quantities with those of observations to evaluate the underlying assumptions of the model. We then examined unobserved entities for trends imposed by the sorting and selection process. Variables that are unimportant in determining the declining trend in $Z_{SD} \cdot K_d$(PAR) should retain a random distribution with surrogate time, while important variables will display increasing or decreasing trends of varying strengths. This approach allows for patterns such as time-varying upper or lower bounds to be discerned that are not well described by simple correlation coefficients.

[34] Probability distributions and associated parameters of the random variables assigned to concentrations and parameters in the bio-optical model are given in Table 3. We allowed θ to vary over a wide enough range (30 to 100 mg C [mg CHLA]$^{-1}$) that $b_p^\phi(\lambda)$ (equation (16)) can be taken to represent scattering by phytoplankton and large organic detritus. Although the procedure produced many combinations of concentrations that did not match any observed region, the 60,000 simulations gave sufficient numbers of realizations after selecting for ranges matching observations in the different segments of the Bay. The ranges of observed variables, intended to match the ranges of annual averages ±1 standard deviation, used to select simulations for the different segments of the Bay are given in Table 4. We assigned simulations to a year class by matching simulated $Z_{SD} \cdot K_d$(PAR) to that predicted by the linear regression of observed $Z_{SD} \cdot K_d$(PAR) against year. In this way, the observed data determine which simulations are relevant to a

Table 4. Ranges of Observed Variables Used to Select Simulations for Different Segments of Chesapeake Bay[a]

Measurement (Units)	Upper Bay Minimum, Maximum	Middle Bay Minimum, Maximum	CB4MH Minimum, Maximum
$R_{rs}(555)$ (sr^{-1})	0.004, 0.012	0.005, 0.011	0.004, 0.010
CHLA (mg m^{-3})	4.0, 32.0	2.0, 26.0	4.0, 18.0
TSS (g m^{-3})	2.0, 20.0	2.0, 20.0	3.0, 9.0
Z_{SD} (m)	0.6, 2.2	1.3, 3.0	1.3, 2.3
K_d(PAR) (m^{-1})	0.6, 2.4	0.4, 1.5	0.7, 1.2

[a]Segment boundaries are defined in text. CB4MH is the Chesapeake Bay Water Quality Monitoring Program segment closest to IOP measurements made by *Tzortziou et al.* [2006]. The ranges were chosen to encompass the minimum and maximum observed annual means ±1 standard deviation, except for $R_{rs}(555)$, which encompass observed monthly composites from 1998 to 2009.

particular region (Table 4), and where they fall in surrogate time. The strength of the underlying relationships between AOPs and IOPs embodied in equation (2) and its dependencies determines which parameters emerge as important in determining a trend in $Z_{SD} \cdot K_d$(PAR). Wider ranges for the concentrations in Table 3 would produce a greater number of simulations not meeting the criteria of Table 4, and wider ranges for the optical parameters have little support in the literature.

[35] In the auxiliary material we demonstrate the inadequacy of a null model, in which mass-specific IOPs were considered constant and only concentrations of CDOM, CHLA, and TSS were varied, to reproduce observed patterns in the data. Additionally, in the auxiliary material we examine the sensitivity of the overall conclusions to uncertainty in the proportionality between $R_{rs}(555)$ and $b_b/(a + b_b)$ and to alternative formulations of scattering by phytoplankton.

5. Results

5.1. In Situ Measurements

[36] Annual averages of the $Z_{SD} \cdot K_d$(PAR) product declined steadily since the inception of measurements in the midmesohaline (upper and mid bay, measured since 1985) and polyhaline (lower Bay, measured since 1993) portions of Chesapeake Bay (Figure 3a). GLM analysis of $Z_{SD} \cdot K_d$(PAR) revealed that $Z_{SD} \cdot K_d$(PAR) declined significantly in all segments (Table 5). The greatest rate of decline was in the mesohaline mid-Bay. Examination of the Z_{SD} and K_d(PAR) factors separately revealed that the trend in the product was driven primarily by declines in Secchi depth, which had significantly negative slopes in all of the segments (Figure 2 and Table 5). In contrast, the slopes of regressions of K_d(PAR) versus year were insignificant in upper Bay and tidal fresh/oligohaline segments, significantly negative in lower Bay, and weakly positive (the wrong direction to account for the trend in the $Z_{SD} \cdot K_d$(PAR) product) in the middle Bay (Table 5). The implications of these changes for the relationship between K_d(PAR) and Z_{SD} are shown in Figure 3b for mesohaline upper Bay segment. Deeper Secchi depths, including 3 measurements ≥ 2.0 m, were observed early in the monitoring period (1985–1988), compared with a maximum of 1.7 m from 2007 to 2008 (Figure 3b). At comparable Secchi depths from 1.0 to 1.5 m, higher values of K_d(PAR) were more often observed from 1985 to 1988 than during the later period (Figure 3b). Restricting the analysis reported in Table 5 to years for which SeaWiFS data are available (1997–2009, not shown) yielded very similar results; that is, the slopes for $Z_{SD} \cdot K_d$(PAR) and Z_{SD} versus year were significantly negative for all segments, and the slopes for K_d(PAR) were insignificant for all segments but the Middle Bay.

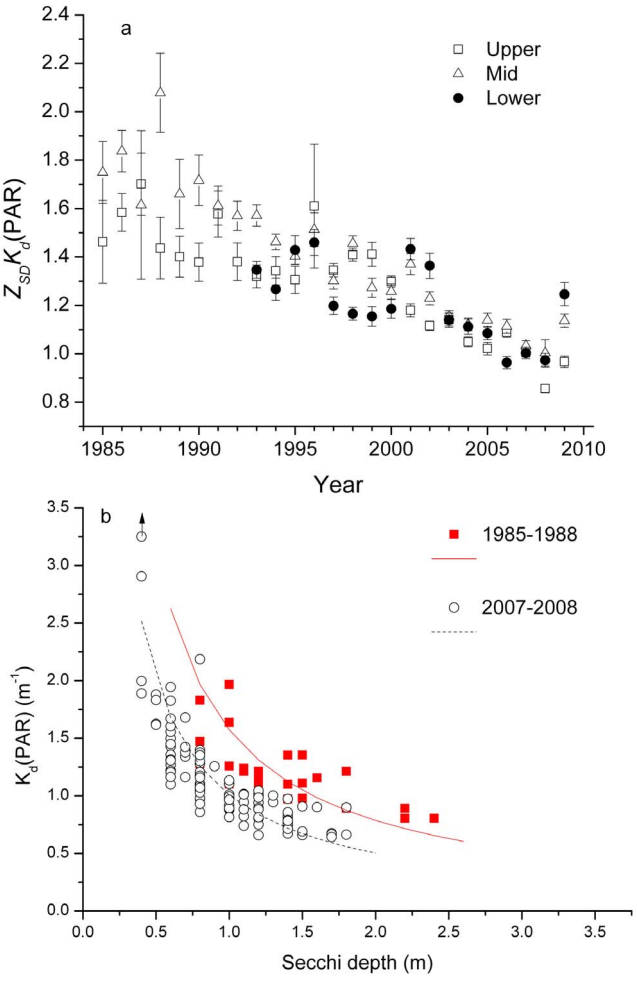

Figure 3. (a) Annual means of the $Z_{SD} \cdot K_d$(PAR) product in the upper (squares), middle (triangles), and lower (filled circles) segments of Chesapeake Bay. Error bars are ±1 standard error. (b) Relationship of K_d(PAR) to Z_{SD} in the upper Bay segment measured early in the monitoring record (1985–1988, red squares and solid line) compared with recent measurements (2007–2008, black circles and dotted line). Higher Secchi depths at comparable diffuse attenuation coefficients were measured early in the record compared with recent measurements.

Table 5. Slopes of Secchi Depth (Z_{sd}), Diffuse Attenuation Coefficient for PAR, (K_d(PAR)), and the $Z_{SD} \cdot K_d$(PAR) Product Against Year in Main Stem Segments of Chesapeake Bay[a]

Segment	$Z_{SD} \cdot K_d$(PAR) (yr^{-1}) (SE)	Z_{sd} (m yr^{-1}) (SE)	K_d(PAR) (m^{-1} yr^{-1}) (SE)
TF/OH	−0.0268 (0.0020)	−0.0061 (0.0018)	−0.0118 (ns)
Upper	−0.0288 (0.0016)	−0.0177 (0.0022)	−0.0052 (ns)
Middle	−0.0329 (0.0015)	−0.0277 (0.0018)	0.0062 (0.0010)
Lower	−0.0205 (0.0019)	−0.0226 (0.0022)	−0.0043 (0.0012)

[a]Standard errors (SE) are given in parentheses; ns, not significant ($P \geq 0.05$). Data were available from 1985 to 2009 for tidal fresh, oligohaline, and upper and mid-Bay segments in Maryland and from 1993 to 2009 for middle and lower Bay segments in Virginia. Segment boundaries defined in text.

5.2. Remote Sensing Measurements

[37] Based on theoretical analysis (Figure 1a), the declining trends in $Z_{SD} \cdot K_d$(PAR) imply that the b/a ratio has nearly doubled, from 6 to 12, in wave bands that govern Secchi disk visibility in Chesapeake Bay, which we take to be near 555 nm [*Tzortziou et al.*, 2006]. Based on equation (1), an increasing b/a ratio implies the possibility that a change in surface brightness might be detectable by satellite, depending on the trajectory of b_b (Figure 1b). GLM analysis of monthly composite R_{rs}(555) from SeaWiFS (available from 1998 through 2008) revealed no significant trends ($P > 0.2$ for all segments). MODIS data R_{rs}(547), available from mid-2002 through 2008, confirm the SeaWiFS results (Figure 4). These observations imply that the increase in the b/a ratio has been accompanied by a corresponding decline in the particulate backscattering ratio, $\tilde{b}_{bp}$(555), such that the total backscattering coefficient has remained stationary.

6. Simulation Results

[38] We demonstrate the modeling process using simulations selected to meet the criteria for midbay observations. Observed $Z_{SD} \cdot K_d$(PAR) data from the midbay segment

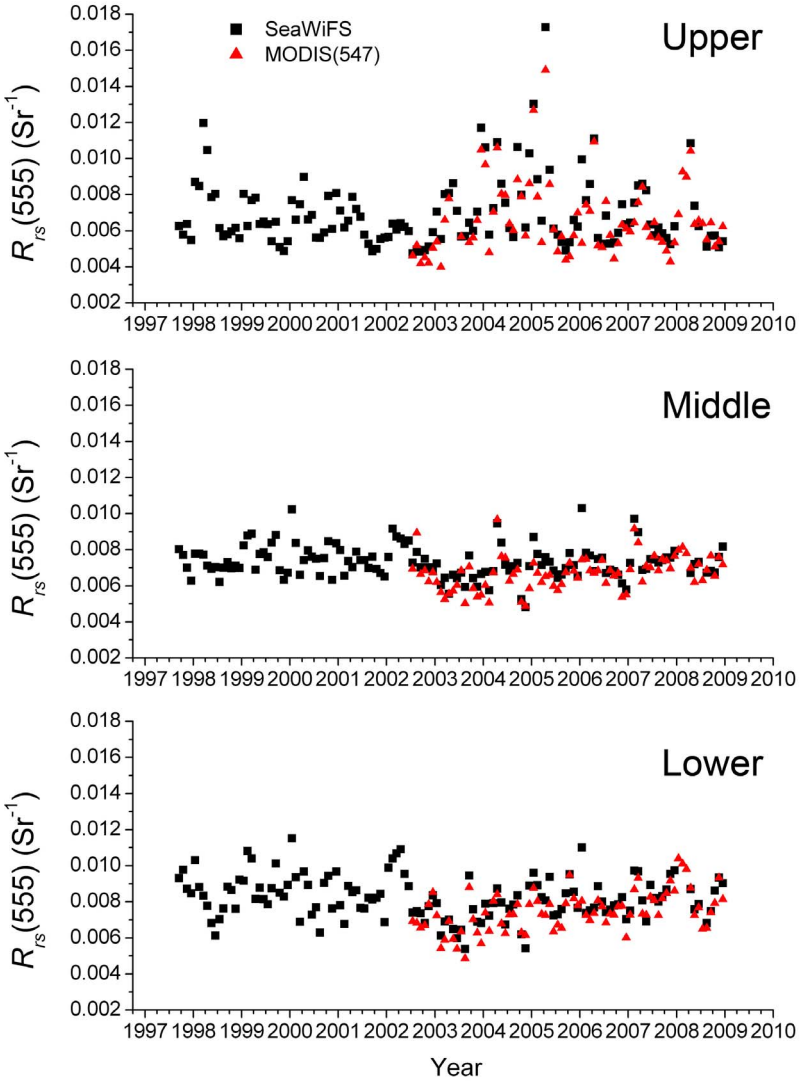

Figure 4. Time series of monthly composite remote sensing reflectance at 555 nm in the upper, middle, and lower regions of Chesapeake Bay measured by SeaWiFS (black squares) and MODIS-Aqua satellites (red triangles). MODIS measurements are centered at 547 nm, the closest comparable wave band.

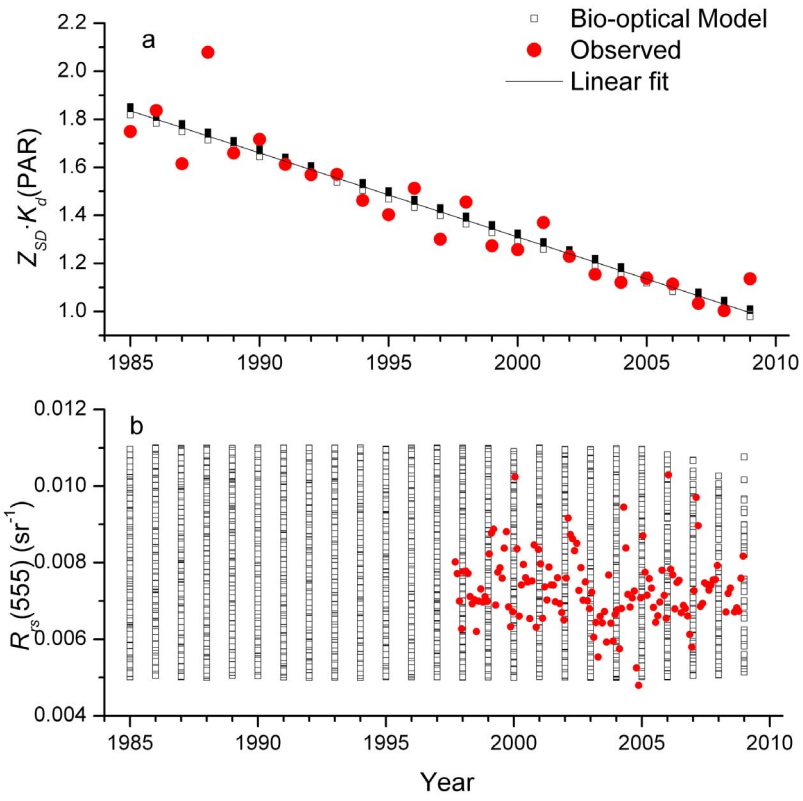

Figure 5. (a) Observed annual averages (red circles) of the $Z_{SD} \cdot K_d$(PAR) product at mesohaline mid-Bay segment and values simulated by the bio-optical model with variable mass-specific inherent optical properties (scenario 1, black squares). Simulated data were sorted on $Z_{SD} \cdot K_d$(PAR) descending and selected to coincide with the observed range for the middle Bay (Table 4). A linear fit to observed data (black line) was used to bin the simulations into years. (b) Remote sensing reflectance at 555 nm simulated by the bio-optical model with variable mass-specific IOPs (black squares). Sorting the data on $Z_{SD} \cdot K_d$(PAR) descending imposed no increasing trend on the simulated remote sensing reflectance, in agreement with observations. Red circles are monthly composites of SeaWiFS data (see Figure 4).

were fit by a line given by $Z_{SD} \cdot K_d$(PAR) = 1.835–0.035 (year 1985) (Figure 5a). The model results were sorted by simulated $Z_{SD} \cdot K_d$(PAR) in descending order. Each simulation falling within the ranges given in Table 4 (middle column) was assigned a year value on the basis of its simulated $Z_{SD} \cdot K_d$(PAR) value by rearrangement of the linear fit of $Z_{SD} \cdot K_d$(PAR) to year, and rounding to the nearest integer. We first examined patterns in the simulations that can be compared with measurements. We then examined variations in the mass-specific IOPs and components of the four-component particulate model for "temporal" patterns to determine the component(s) most likely responsible for observed changes in $Z_{SD} \cdot K_d$(PAR).

6.1. Scenario 1

[39] Allowing variations in the mass-specific IOPs in equations (14b), (16), and (17) (Table 3) produced simulations that were broadly compatible with measurements of $Z_{SD} \cdot K_d$(PAR) and R_{rs}(555) (Figures 5a and 5b). Sorting the simulations on $Z_{SD} \cdot K_d$(PAR) imposed no increasing trend in R_{rs}(555) (Figure 5b). Moreover, the complete range of observed R_{rs}(555) can occur in all of the simulated years for which measurements are available.

[40] A wide range of chlorophyll concentrations was compatible with the declining trend in $Z_{SD} \cdot K_d$(PAR) (Figure 6a). Observed annual means and standard deviations of chlorophyll concentrations were within the ranges of the simulation for every year but the last year considered, 2009. There was a decrease in the upper bound of compatible simulations beginning about simulated year 2001, indicating that $Z_{SD} \cdot K_d$(PAR) less than about 1.2 begins to constrain the compatible chlorophyll concentrations.

[41] The high values of $Z_{SD} \cdot K_d$(PAR) early in the record admit Secchi depths as high as 2.6 m, while the lower values near the end of the record restrict compatible Secchi depths to <1.6 m (Figure 6b). The sorting thus imposed a declining trend in Z_{SD} consisting of a declining lower bound from 1985 to 1995 and declining upper bound from 1997 to 2009. Observations of annual mean Z_{SD} in that segment generally fell within the bounds of the simulations in all but the last year (Figure 6c).

[42] Sorting on $Z_{SD} \cdot K_d$(PAR) imposed a trend of widening permitted values of simulated K_d(PAR) from 1985 to 1995, followed by a declining trend in the upper bound from 1995 onward (Figure 6c). Over the entire period the trend in simulated K_d(PAR) was weaker than that of Z_{SD},

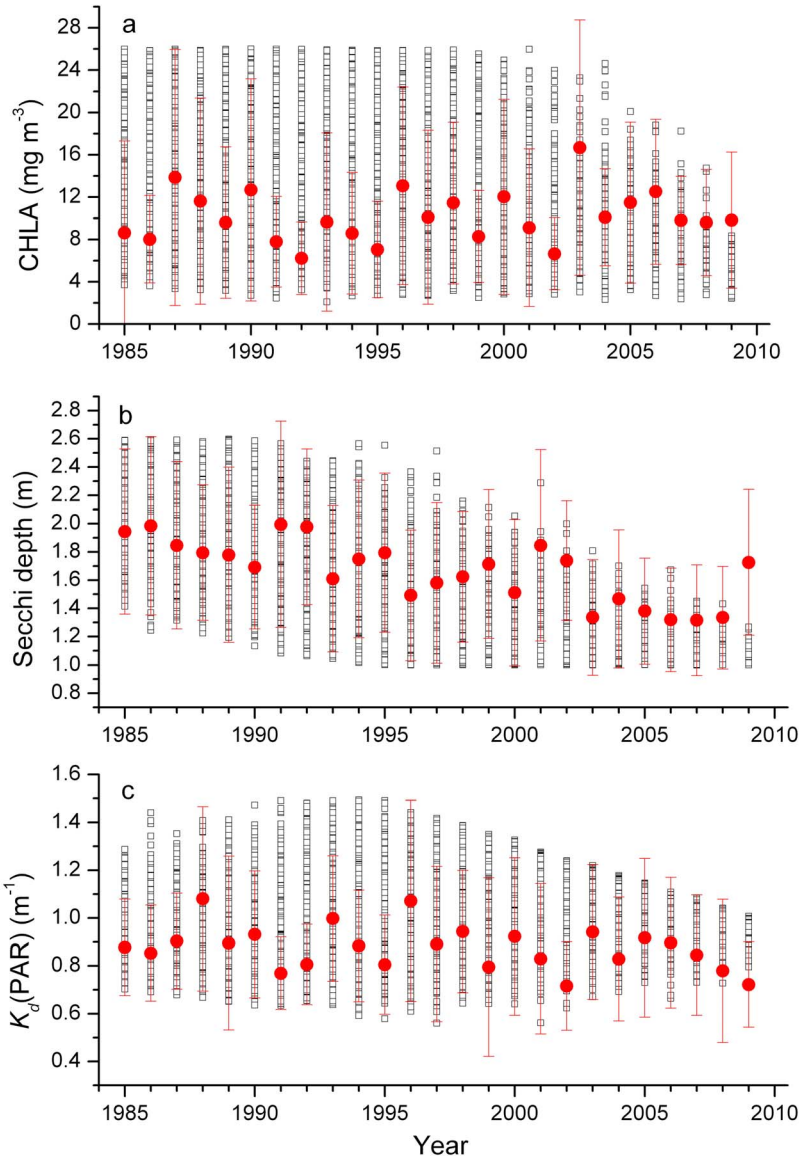

Figure 6. (a) Simulated chlorophyll *a* concentrations (black squares) from scenario 1 in which mass-specific IOPs were varied as given in Table 3. Simulated output was sorted on $Z_{SD} \cdot K_d$(PAR) descending and selected according to mid-Bay ranges given in Table 4. Red circles are annual averages of measurements made by the Chesapeake Bay Water Quality Monitoring Program. As in Figure 6a for (b) Secchi depth and (c) K_d(PAR). Error bars are ±1 standard deviation.

consistent with the measurements (Figures 6b and 6c and Table 5).

[43] To examine variations in the simulated mass-specific IOPs we sorted and selected the data to match observations near the location of the measurements made in 2002 by *Tzortziou et al.* [2006] (Table 4, CBP segment CB4MH). Of the four specific IOPs varied randomly in scenario 1, the particulate backscattering ratio, $\tilde{b}_{bp}(555)$, had the strongest trend imposed by sorting on $Z_{SD} \cdot K_d$(PAR) descending (Figure 7a). $Z_{SD} \cdot K_d$(PAR) values lower than 1.2 as observed in recent years require $\tilde{b}_{bp}(555)$ to be <0.02, whereas $Z_{SD} \cdot K_d$(PAR) values as high as 2 as observed early in the record admit a wide range of $\tilde{b}_{bp}(555)$ between 0.015 and 0.035 (Figure 7a). The annually averaged $\tilde{b}_{bp}(555)$ of 0.0128 measured in 2002 by *Tzortziou et al.* [2006] fell well within compatible simulations for that simulated year, but would be well below the average of simulations early in the record (Figure 7a).

[44] The trends imposed on $b_p^*(555)$ and $a_\phi^*(675)$ were weaker than that of $\tilde{b}_{bp}(555)$ (Figures 7b and 7c). A wide range for these parameters was generally compatible with the observed trend in $Z_{SD} \cdot K_d$(PAR) throughout the period, with the trend occurring as an increasing lower bound from simulated 1996 onward (Figures 7b and 7c). Measurements of $b_p^*(555)$ and $a_\phi^*(675)$ in 2002 (data from *Tzortziou et al.* [2006]) were near the lower bound and middle of compatible simulated values, respectively (Figures 7b and 7c).

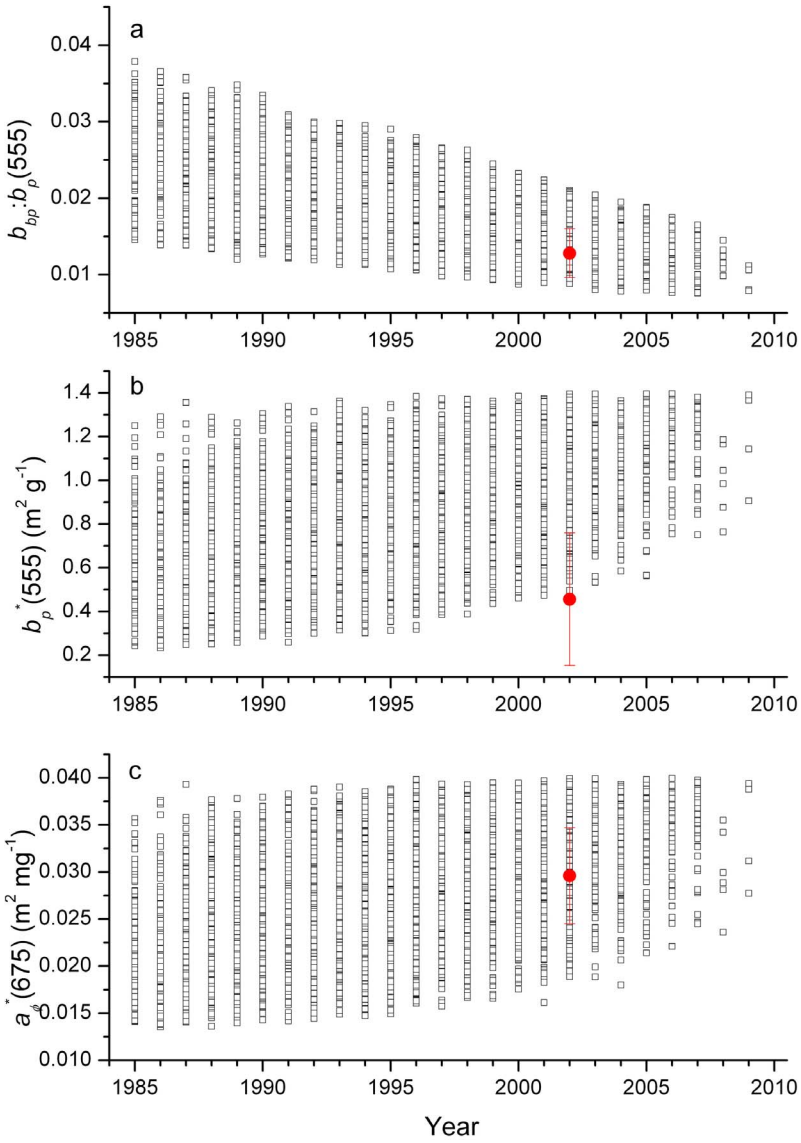

Figure 7. Inherent optical properties (black squares) used in scenario 1, sorted on simulated $Z_{SD} \cdot K_d$(PAR) descending and selected according to ranges for Chesapeake Bay Program segment CB4MH (Table 4). Red circles are measurements from *Tzortziou et al.* [2006]. (a) Particulate backscattering ratio, (b) mass-specific scattering coefficient of suspended particulate matter, and (c) specific absorption coefficient of phytoplankton chlorophyll at 675 nm. Error bars are ±1 standard deviation of measurements.

6.2. Scenario 2

[45] The second scenario utilized the four-component NAP model. Patterns of simulated $R_{rs}(555)$, Z_{SD}, K_d(PAR), and $Z_{SD} \cdot K_d$(PAR) as well as the derived bulk mass-specific absorption and scattering coefficients with simulated time with this model were very similar to those obtained with scenario 1 (not shown). The separate components of the particulate model are not individually measureable. Measurable quantities calculated from the particulate submodel, *POM* and f_{org} were measured by CBP for short subsets of the monitoring period (Figure 8). Simulated data were sorted and selected according to CBP segment CB4MH for comparison with these few measurements. Sorting the simulations on $Z_{SD} \cdot K_d$(PAR) descending imposed a strong increasing trend on calculated *POM* (Figure 8a). *POM* was measured the first 3 years of the monitoring program. Annual mean values for 1 of the 3 years was higher than compatible values determined by the simulation, but the measurements were highly variable and the other 2 years fell within the range of simulations (Figure 8a). Measurement of f_{org} was instituted for the mesohaline mid-Bay in 2001. Measured annual means of f_{org} fell within the range of compatible simulations and showed an increasing trend similar to that imposed on the simulations by sorting on $Z_{SD} \cdot K_d$(PAR) (Figure 8b).

[46] Of the four components of the NAP pool, sorting on $Z_{SD} \cdot K_d$(PAR) imposed the strongest trend on the small

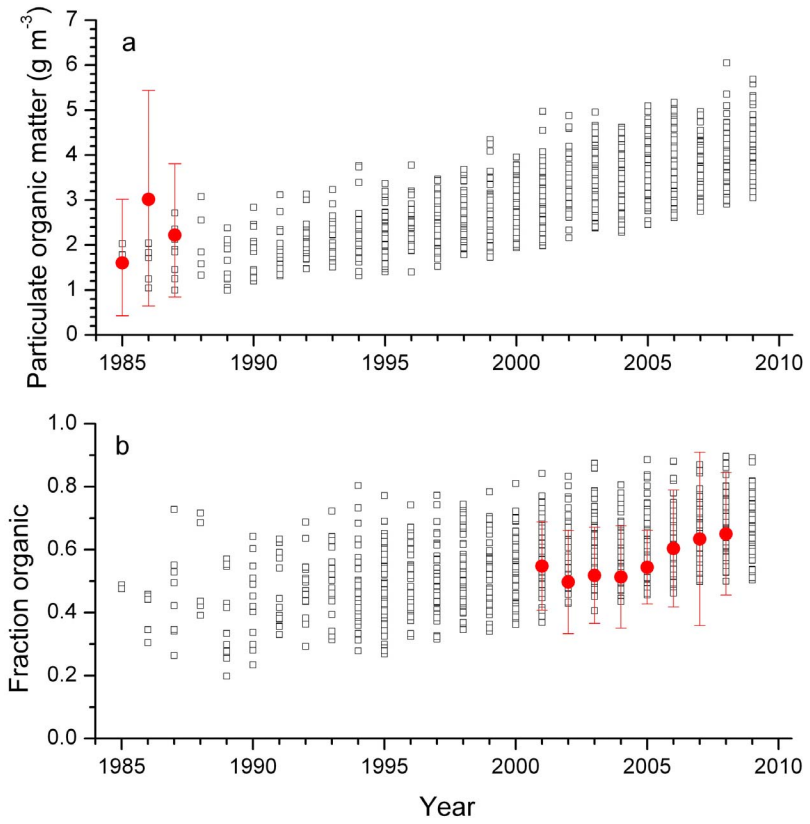

Figure 8. Derived quantities calculated from the four-component particulate NAP model (black squares) that are amenable to measurement. Simulated quantities were sorted on $Z_{SD} \cdot K_d$(PAR) descending and selected according to ranges observed for Chesapeake Bay Program segment CB4MH (Table 4). (a) Particulate organic matter and (b) fraction of total suspended solids that is organic. Measured annual means (red circles) are only available for restricted portions of the monitoring period. Error bars around measured points are ±1 standard deviation.

organic detritus pool (Figure 9a). Large organic detritus displayed an increasing trend in its upper bound (Figure 9b), but a wide range of concentrations was compatible with declining $Z_{SD} \cdot K_d$(PAR) over most of the observation period. The pattern imposed on small mineral particulates resembled that of K_d(PAR) (cf. Figures 9c and 6d), having a range that increased over the first decade of the simulation, and a declining upper bound after simulated year 1996. The restriction of the upper bound early in the record is due to incompatibility of small minerals with the higher Z_{SD} observed early in the record [*Swift et al.*, 2006], while the declining upper bound after 1996 is a necessary consequence of the declining backscattering ratio (Figure 7a). The full range of assumed values for large mineral particulates was compatible with the downward trend in $Z_{SD} \cdot K_d$(PAR) (Figure 9d), due to the overall low concentration range assumed for this component (Table 3).

7. Discussion and Conclusions

[47] A long-term trend of declining value of the $Z_{SD} \cdot K_d$(PAR) product was observed in Chesapeake Bay that was significant in all segments examined (Table 5). This indicates an increase from some source of particle loading relative to color loading [*Koenings and Edmundson*, 1991], and that the optical depth at the Secchi depth has declined. Water clarity in the Bay is frequently linked to flow of the Susquehanna River [*Harding*, 1994], but there has been no long-term trend in flow and the declining trend in $Z_{SD} \cdot K_d$(PAR) has persisted through high- and low-flow years (Figure 3). According to the theory, declining $Z_{SD} \cdot K_d$(PAR) implies an increase in the scattering-to-absorption ratio in wave bands that govern Secchi disk visibility. If this change were taking place with a stationary backscattering ratio then remote sensing reflectance would necessarily have an increasing trend (Figure 1b), according to equation (1) [*Lee et al.*, 1994]. This has not been the case (Figure 4), which leads us to conclude that the backscattering ratio has, on average, declined over the observation period (Figure 1b).

[48] Scenario 1 in which mass-specific IOPs, concentrations of LAS, and the backscattering ratio were allowed to vary independently made no assumptions about the identity of substances that are responsible for the declining trend in $Z_{SD} \cdot K_d$(PAR). The approach taken with the bio-optical model allowed trends and ranges of observed entities to arrange and constrain values of parameters for which no or

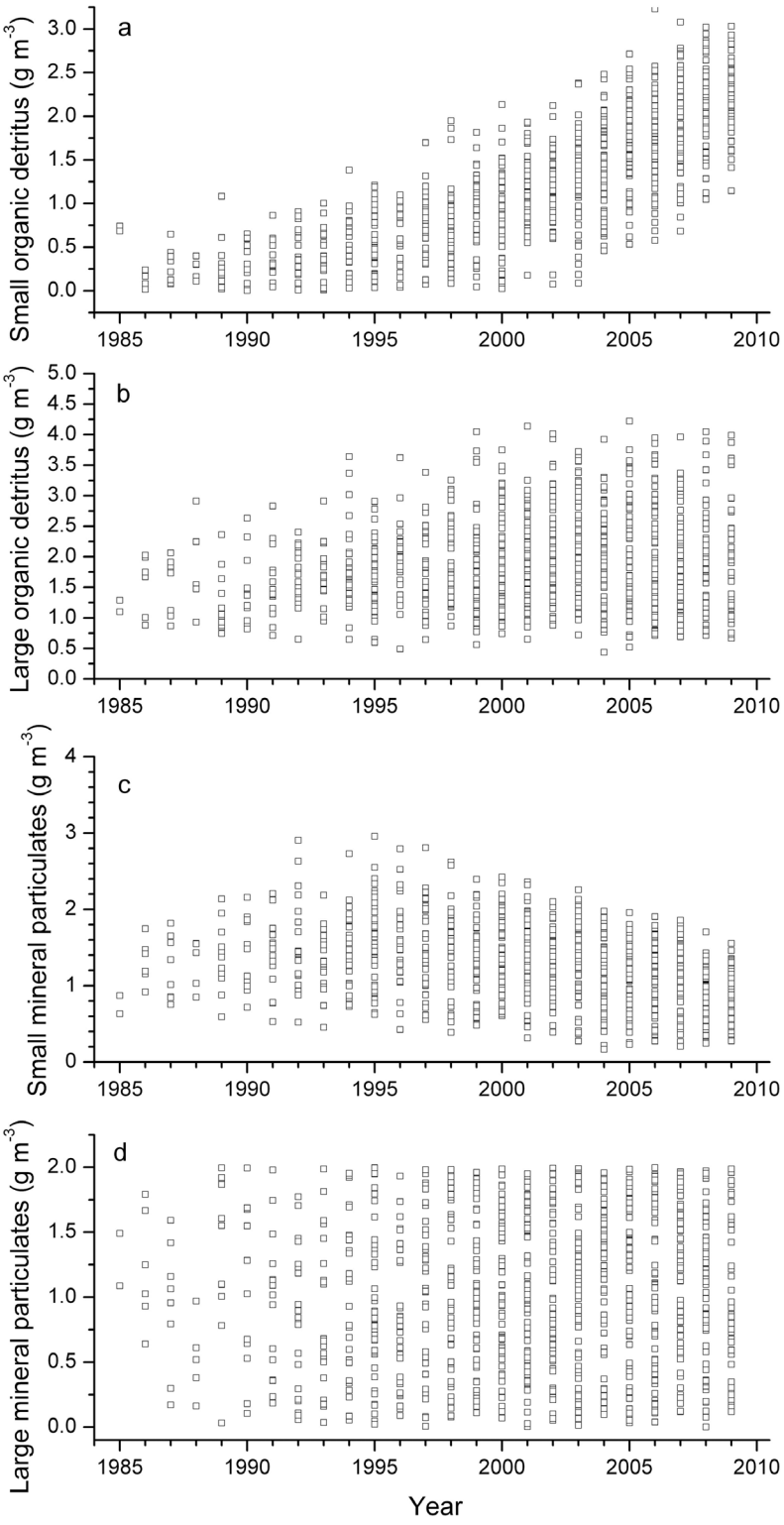

Figure 9. Components of the nonalgal particulate model sorted on simulated $Z_{SD} \cdot K_d$(PAR) descending and selected according to ranges observed for Chesapeake Bay Program segment CB4MH (Table 4). (a) Small organic detritus, (b) large organic detritus, (c) small mineral particulates, and (d) large mineral particulates.

few observations are available. That analysis confirmed that a decreasing backscattering ratio was the most important condition determining a decreasing $Z_{SD} \cdot K_d$(PAR) subject to a stationary R_{rs}(555) (Figure 7a). Increasing b_p*(555) and a_ϕ*(675) were also potentially implicated (Figures 7b and 7c).

[49] In scenario 2 we attempted to assemble the mass-specific IOPs and backscattering ratio from variations in the relative amounts of broad classes of particles that have been investigated empirically and theoretically [*Babin et al.*, 2003a, 2003b; *Stramski et al.*, 2001]. Based on the results of scenario 1 it could be anticipated that sorting on $Z_{SD} \cdot K_d$(PAR) descending would favor increasing concentrations of particles having relatively low $\tilde{b}_{bp}$(555) and high b_p*(555), which we ascribed to organic particulates, and small detritus in particular (Table 2) [*Stramski et al.*, 2001]. The high backscattering efficiency of small mineral particles means that the low $Z_{SD} \cdot K_d$(PAR) values observed in recent years are incompatible with increasing concentrations of these particles (Figure 9c). The failure of the simulated concentrations of large mineral particles to diverge from the parent distribution (Figure 9d) indicates that the dynamics of large minerals were unrelated to observed trends in $Z_{SD} \cdot K_d$(PAR).

[50] Additional simulations reported in the accompanying auxiliary material demonstrate that the conclusions of the modeling are very robust with respect to changes in model structure. For example, holding mass-specific IOPs (including $\tilde{b}_{bp}$(555)) constant and varying only concentrations of LAS in simulation 1 imposed an increasing trend on R_{rs}(555), contrary to observations (Figure 4). Allowing reasonable variability in the proportionality constant in equation (1) imposed the same decreasing trend on $\tilde{b}_{bp}$(555) as in Figure 7a, albeit with wider limits. Formulation of the scattering by phytoplankton in terms of CHLA rather than carbon according to relationships of *Huot et al.* [2008] produced results very similar to Figure 9. These additional simulations indicate that the observations demand a decreasing particulate backscattering ratio, and that the modeling strongly support changes in the optical properties of particulate matter that we have formulated as increasing concentrations of small organic detritus.

[51] Particulate matter in natural waters frequently exists in large, loosely bound aggregates held together by sticky transparent exopolymeric particles (TEP) excreted by phytoplankton and bacteria [*Passow*, 2002]. There have been relatively few studies of the optical properties of large fragile aggregates. *Berthon et al.* [2000] measured large increases in the b/a ratio during mucilage events in the northern Adriatic Sea, but they did not have accompanying measurements of backscattering ratio. Surface reflectance spectra at all but one station associated with mucilage events were slightly lower than the average measured during profiles not associated with mucilage events, indicating a probable decrease in $\tilde{b}_{bp}(\lambda)$ due to the mucilage events. *Boss et al.* [2009] observed an increase in the beam attenuation cross section and the backscattering fraction when large aggregates were disrupted by shear. An increasing tendency in Chesapeake Bay for the particulate matter to occur in large aggregates might produce a compatible declining trend in $\tilde{b}_{bp}$(555) (Figure 7a), but a concomitant trend toward decreasing b_p*(555) as implied by the observations of *Boss et al.* [2009] would be in the wrong direction (Figure 7b). Nevertheless, the dependence of the declining trend in $Z_{SD} \cdot K_d$(PAR) on $\tilde{b}_{bp}$(555) is stronger than on b_p*(555) (Figures 7a and 7b). Taken together, a large increase in b/a [*Berthon et al.*, 2000] and reduction in $\tilde{b}_{bp}$ [*Boss et al.*, 2009] associated with an increased prevalence of large aggregates caused by increasing concentrations of TEP could have the effect on optical properties needed to generate the observed trend in $Z_{SD} \cdot K_d$(PAR) without producing a concomitant increasing trend in R_{rs}. We speculate that alternating sedimentation and resuspension of TEP and aggregated material [*Azetsu-Scott and Passow*, 2004] could possibly accumulate TEP within the system and produce a long-term trend in the b/a ratio.

[52] As formulated in scenario 2, increasing concentrations of small organic particles had the strongest association with the declining trend in $Z_{SD} \cdot K_d$(PAR) (Figure 9a). The observed trend in $Z_{SD} \cdot K_d$(PAR) also required a declining trend in particles with optical properties that we assigned to small minerals (Figure 9c), owing to the strong backscattering cross section of small minerals [*Stramski et al.*, 2001]. That is, an increase in the b/a ratio without an increasing trend in R_{rs}(555) (Figure 4) demands a declining trend in the upper bound of small minerals. Here again we emphasize that it is the optical effect that is the requisite factor. Increased packaging of the small mineral particulates into aggregates with smaller mass-specific backscattering cross sections without declines in mass concentrations is also compatible with the observations.

[53] Definitive determination of the cause in the declining trend in $Z_{SD} \cdot K_d$(PAR) is not possible with the available data. There are surprisingly few measured parameters available for comparison with predictions of the bio-optical model. For example, *POM* was measured early in the monitoring program but analyses were dropped after 3 years (Figure 8a). The bio-optical model predicts that current levels of *POM* should be significantly higher than during the first 3 years of the record, due to changes in the organic detritus, particularly the small fraction. Similarly, measurements of f_{org} were only instituted in 2001 for the Maryland portion of the Bay (Figure 8b). The increasing pattern is intriguingly similar to predictions of the bio-optical model, but the range of compatible values is wide enough over the entire monitoring period that current levels would not have to be higher than at the inception of the monitoring. IOPs have never been part of the routine monitoring in Chesapeake Bay, but simulation 2 indicates that b_p*(555) (Figure 7b) might now be higher than when measured by *Tzortziou et al.* [2006]. Results of simulation 1 indicated that backscattering ratios should be lower now than in the 1980s, but changes since 2002 would not likely be detectable (Figure 7a).

[54] Known long-term trends that have been documented for Chesapeake Bay do not have optical signals in themselves. For example, temperature, shown to have a warming trend of ~0.16 to 0.21°C per decade [*Preston*, 2004], has only a small effect on pure water absorption at near-infrared wavelengths [*Pegau et al.*, 1997] which, by itself, could not affect $Z_{SD} \cdot K_d$(PAR) as observed. Similarly, relative sea level rise of about 3 mm yr^{-1} (variable with location)

[*Zervas*, 2009] would by itself have no effect on Z_{SD} or K_d(PAR). To affect $Z_{SD} \cdot K_d$(PAR) these long-term trends would need to contribute to qualitative changes in the particulate matter via ecosystem processes such as changes in the size structure of plankton populations and the detritus derived from them, or physical processes affecting sediment resuspension and aggregation.

[55] In Chesapeake Bay the interconversion between Secchi depth and K_d(PAR) has never been very precise in any given year (Figure 3b), and the long-term declining trend in $Z_{SD} \cdot K_d$(PAR) adds an additional source of uncertainty to any attempted conversion. Associated errors will affect calculations of phytoplankton primary production [*Lewis et al.*, 1985] and assessment of light availability for SAV [*Kemp et al.*, 2004]. Calculations of ecosystem processes that require a quantitative estimate of light flux should be based on measurements of irradiance. We agree with *Effler* [1985] that when circumstances require use of K_d(PAR) estimated from Z_{SD}, the calculation be accompanied by error sensitivity with broad limits, e.g., ±0.7, on $Z_{SD} \cdot K_d$(PAR).

[56] This is not to say that the Secchi depth measurement is without value. As a simple visual measure of water transparency, Z_{SD} may be a better indicator of, e.g., reactive distance for predatory fish, than K_d(PAR) [*Benfield and Minello*, 1996]. Indeed, there would have been no indication that long-term changes in optical properties are taking place in Chesapeake Bay from measurements of K_d(PAR) alone (Figure 6c and Table 5). The last measurements considered (2009) indicate that the trend may be leveling or reversing (Figure 6b), so that continued measurement of Z_{SD} is advisable.

[57] The observation of a declining trend in Z_{SD} (Figure 6b) without a concomitant trend in $R_{rs}(555)$ (Figure 4) casts doubt on the feasibility of developing a reliable Secchi depth product for Chesapeake Bay based on satellite remote sensing data. Secchi depth is most sensitive to b/a, while R_{rs} depends on b_b/a. Estimation of b from remote sensing measurements requires knowledge of the backscattering ratio. These results indicate that assumption of a stationary $\tilde{b}_{bp}$ for Chesapeake Bay is not robust. In contrast, remote estimation of K_d(PAR) should be reliable due to its dependence on $a(\lambda)$ and the magnitude of backscattering, $b_b(\lambda)$, rather than the backscattering ratio (equation (5)).

[58] The tandem use of remote sensing and in situ data was, however, indispensible for constraining possible causes of the $Z_{SD} \cdot K_d$(PAR) trend. A bio-optical model based solely on changes in concentrations of light attenuating substances was unable to satisfy the simultaneous requirements of both declining $Z_{SD} \cdot K_d$(PAR) and stationary $R_{rs}(555)$ (see auxiliary material). Changes in mass-specific IOPs were necessary to accommodate both in situ and remotely sensed data. Any more definitive cause for the declining trend in $Z_{SD} \cdot K_d$(PAR) could not be identified with available data. Resumption of *POM* measurements could provide valuable insight, as would further studies to better characterize the source of optical variability in NAP. If the trend is caused by changes in the relative amounts of organic versus inorganic suspended solids, then present concentrations of POM should be higher on average than from 1985 to 1987 (Figure 8a). Measurements can now be made that would implicate the alternative explanation, i.e., increases in TEP [*Wetz et al.*, 2009] and formation of large fragile aggregates [*Flory et al.*, 2004], though retrospective analysis is not possible.

Notation

$a(\lambda)$ Absorption coefficient (m^{-1}).
$a_g(\lambda)$ Absorption coefficient of colored dissolved organic matter (m^{-1}).
$a_{NAP}(\lambda)$ Absorption coefficient of nonalgal particles (m^{-1}).
AOPs Apparent optical properties.
$a_p(\lambda)$ Absorption coefficient of particles (m^{-1}).
$a_w(\lambda)$ Absorption coefficient of water (m^{-1}).
$a_x^*(\lambda)$ Specific absorption coefficient of component x of nonalgal particles ($m^2\ g^{-1}$).
$a_\phi(\lambda)$ Absorption coefficient of phytoplankton (m^{-1}).
$\tilde{b}_b(\lambda)$ Backscattering to total scattering ratio (dimensionless).
$\tilde{b}_{bw}$ Backscattering ratio of water (dimensionless).
$\tilde{b}_{b\phi}$ Backscattering ratio of phytoplankton (dimensionless).
$\tilde{b}_{bp}$ Backscattering ratio of particles (dimensionless).
$\tilde{b}_{bx}$ Backscattering ratio by component x of nonalgal particles (dimensionless).
$b(\lambda)$ Scattering coefficient (m^{-1}).
$b_b(\lambda)$ Backscattering coefficient (m^{-1}).
$b_{bNAP}(\lambda)$ Backscattering coefficient of nonalgal particles (m^{-1}).
$b_{bw}(\lambda)$ Backscattering coefficient of water (m^{-1}).
$b_{b\phi}(\lambda)$ Backscattering coefficient of phytoplankton (m^{-1}).
$b_{NAP}(\lambda)$ Scattering coefficient of nonalgal particles (m^{-1}).
$b_p^\phi(\lambda)$ Particulate scattering coefficient of phytoplankton (m^{-1}).
$b_w(\lambda)$ Scattering coefficient of water (m^{-1}).
$b_x^*(\lambda)$ Specific scattering coefficient of component x of nonalgal particles ($m^2\ g^{-1}$).
$b_\phi(\lambda)$ Scattering coefficient of phytoplankton (m^{-1}).
$b_\phi^*(\lambda)$ Specific scattering coefficient of phytoplankton ($m^2\ mg^{-1}$).
$c(\lambda)$ Beam attenuation coefficient (m^{-1}).
C_0 Apparent contrast between the Secchi disk and the surrounding medium (dimensionless).
c_1^x Specific absorption coefficient of component x of nonalgal particles at long wavelengths ($m^2\ g^{-1}$).
c_2^x Scale factor of specific absorption coefficient of component x of nonalgal particles at reference wavelength ($m^2\ g^{-1}$).
CBP Chesapeake Bay Program.
CDOM Colored dissolved organic matter.
CHLA Chlorophyll *a* ($mg\ m^{-3}$).
C_T Threshold contrast (dimensionless).
D Particle diameter (μm).
$E_0(z)$ Surface-incident cosine-corrected spectral irradiance (μmol quanta $m^{-2}\ s^{-1}\ nm^{-1}$).

$E_d(z, \lambda)$ Downwelling spectral irradiance (μmol quanta m^{-2} s^{-1} nm^{-1}).
f' Bidirectional coefficient (Sr^{-1}).
f_{org} Organic fraction of suspended particulate matter (dimensionless).
$G(\mu_0)$ Function that scales scattering effect on diffuse attenuation (dimensionless).
IOPs Inherent optical properties.
j Logarithmic slope of particle size distribution (dimensionless).
K_d(PAR) Diffuse attenuation coefficient for photosynthetically active radiation(m^{-1}).
$K_d(\lambda)$ Spectral diffuse attenuation coefficient (m^{-1}).
LAS Light attenuating substances.
μ_0 Cosine of in-water solar zenith angle (dimensionless).
MODIS Moderate Resolution Imaging Spectroradiometer.
$N(D)$ Particle size distribution (number per volume).
NAP Nonalgal particles.
NASA National Aeronautics and Space Administration
PAR Photosynthetically active radiation, 400–700 nm.
PAR_0 Cosine-corrected photosynthetically active radiation at the surface, (μmol quanta m^{-2} s^{-1}).
PAR_z Cosine-corrected photosynthetically active radiation at depth z (μmol quanta m^{-2} s^{-1}).
POM Particulate organic matter (g m^{-3}).
R Reflectance, ratio of upwelling to downwelling irradiance (dimensionless).
R_{disk} Reflectance of Secchi disk (dimensionless).
$R_{rs}(555)$ Remote sensing reflectance at 555 nm (Sr^{-1}).
SeaWiFS Sea-viewing Wide Field-of-view Sensor.
s_g Spectral slope coefficient of absorption by CDOM (nm^{-1}).
SPM_ϕ Dry weight of phytoplankton (g m^{-3}).
s_x Spectral slope coefficient of absorption by component x of nonalgal particles (nm^{-1}).
TF/OH Tidal fresh and oligohaline.
TSS Total suspended solids (g m^{-3}).
z Depth (m).
Z_{SD} Secchi depth (m).
$Z_{SD} \cdot K_d$(PAR) Product of Secchi depth times diffuse attenuation coefficient for PAR (dimensionless).
Γ Coupling constant (dimensionless).
$\phi(\lambda)$ Normalized absorption by phytoplankton (dimensionless).
$\phi^*(\lambda)$ Specific absorption coefficient of phytoplankton chlorophyll (m^2 mg^{-1}).
η_x Power law fit to scattering by component x of nonalgal particles (dimensionless).
η_ϕ Power law fit to phytoplankton scattering (dimensionless).
θ Carbon to chlorophyll ratio of phytoplankton (g g^{-1}).
θ_0 Solar incidence angle (°).

[59] **Acknowledgments.** We thank Mike Mallonee for assistance locating POM data. David Bowers and two anonymous reviewers provided constructive comments on an earlier draft.

References

Azetsu-Scott, K., and U. Passow (2004), Ascending marine particles: Significance of transparent exopolymer particles (TEP) in the upper ocean, *Limnol. Oceanogr.*, *49*, 741–748, doi:10.4319/lo.2004.49.3.0741.

Babin, M., and D. Stramski (2002), Light absorption by aquatic particles in the near-infrared spectral region, *Limnol. Oceanogr.*, *47*, 911–915, doi:10.4319/lo.2002.47.3.0911.

Babin, M., A. Morel, V. Fournier-Sicre, F. Fell, and D. Stramski (2003a), Light scattering properties of marine particles in coastal and open ocean waters as related to the particle mass concentration, *Limnol. Oceanogr.*, *48*, 843–859, doi:10.4319/lo.2003.48.2.0843.

Babin, M., D. Stramski, G. M. Ferrari, H. Claustre, A. Bricaud, G. Obolensky, and N. Hoepffner (2003b), Variations in the light absorption coefficients of phytoplankton, nonalgal particles, and dissolved organic matter in coastal waters around Europe, *J. Geophys. Res.*, *108*(C7), 3211, doi:10.1029/2001JC000882.

Benfield, M. C., and T. J. Minello (1996), Relative effects of turbidity and light intensity on reactive distance and feeding of an estuarine fish, *Environ. Biol. Fishes*, *46*, 211–216, doi:10.1007/BF00005223.

Berthon, J.-F., G. Zibordi, and S. B. Hooker (2000), Marine optical measurements of a mucilage event in the northern Adriatic Sea, *Limnol. Oceanogr.*, *45*, 322–327, doi:10.4319/lo.2000.45.2.0322.

Boss, E., M. S. Twardowski, and S. Herring (2001), Shape of the particulate beam attenuation spectrum and its inversion to obtain the shape of the particulate size distribution, *Appl. Opt.*, *40*, 4885–4893, doi:10.1364/AO.40.004885.

Boss, E., W. S. Pegau, M. Lee, M. S. Twardowski, E. Shybanov, and G. Korotaev (2004), Particulate backscattering ratio at LEO 15 and its use to study particle composition and distribution, *J. Geophys. Res.*, *109*, C01014, doi:10.1029/2002JC001514.

Boss, E., W. Slade, and P. Hill (2009), Effect of particulate aggregation in aquatic environments on the beam attenuation and its utility as a proxy for particulate mass, *Opt. Express*, *17*, 9408–9420, doi:10.1364/OE.17.009408.

Bowers, D. G., and C. E. Binding (2006), The optical properties of mineral suspended particles: A review and synthesis, *Estuarine Coastal Shelf Sci.*, *67*, 219–230, doi:10.1016/j.ecss.2005.11.010.

Bowers, D. G., K. M. Braithwaite, W. A. M. Nimmo-Smith, and G. W. Graham (2009), Light scattering by particles suspended in the sea: The role of particle size and density, *Cont. Shelf Res.*, *29*, 1748–1755, doi:10.1016/j.csr.2009.06.004.

Boyce, D. G., M. R. Lewis, and B. Worm (2010), Global phytoplankton decline over the past century, *Nature*, *466*, 591–596, doi:10.1038/nature09268.

Bricaud, A., A. Morel, and L. Prieur (1981), Absorption by dissolved organic matter of the sea (yellow substance) in the UV and visible domains, *Limnol. Oceanogr.*, *26*, 43–53, doi:10.4319/lo.1981.26.1.0043.

Bricaud, A., M. Babin, A. Morel, and H. Claustre (1995), Variability in the chlorophyll-specific absorption coefficients of natural phytoplankton: Analysis and parameterization, *J. Geophys. Res.*, *100*, 13,321–13,332, doi:10.1029/95JC00463.

Chang, G., T. D. Dickey, C. D. Mobley, E. Boss, and W. S. Pegau (2003), Toward closure of upwelling radiance in coastal waters, *Appl. Opt.*, *42*, 1574–1582, doi:10.1364/AO.42.001574.

Clavano, W. R., E. Boss, and L. Karp-Boss (2007), Inherent optical properties of non-spherical marine-like particles—From theory to observation, *Oceanogr. Mar. Biol. Annu. Rev.*, *45*, 1–38, doi:10.1201/9781420050943.ch1.

Davies-Colley, R. J., and W. N. Vant (1988), Estimation of optical properties of water from Secchi disk depths, *Water Resour. Bull.*, *24*, 1329–1335.

Davies-Colley, R. J., W. N. Vant, and D. G. Smith (2003), *Colour and Clarity of Natural Waters: Science and Management of Optical Water Quality*, Blackburn, Caldwell, N. J.

Dennison, W. C., et al. (1993), Assessing water quality with submersed aquatic vegetation, *Bioscience*, *43*, 86–94, doi:10.2307/1311969.

Effler, S. W. (1985), Attenuation versus transparency, *J. Environ. Eng. Div. ASCE*, *111*, 448–459.

Effler, S. W., R. K. Gelda, M. G. Perkins, and D. M. O'Donnell (2005), Modeling light attenuation, Secchi disk, and effects of tripton in Seneca River, New York, USA, *J. Am. Water Resour. Assoc.*, *41*, 971–984.

Effler, S. W., R. K. Gelda, M. G. Perkins, F. Peng, N. G. Hairston Jr., and C. M. Kearns (2008), Patterns and modeling of the long-term optics record of Onondaga Lake, New York, *Arch. Hydrobiol.*, *172*, 217–237, doi:10.1127/1863-9135/2008/0172-0217.

Falkowski, P. G., R. T. Barber, and V. Smetacek (1998), Biogeochemical controls and feedbacks on ocean primary production, *Science*, *281*, 200–206, doi:10.1126/science.281.5374.200.

Flory, E. N., P. S. Hill, T. G. Milligan, and J. Grant (2004), The relationship between floc area and backscatter during a spring phytoplankton bloom, *Deep Sea Res., Part I*, *51*, 213–223, doi:10.1016/j.dsr.2003.09.012.

Gallegos, C. L., R. J. Davies-Colley, and M. Gall (2008), Optical closure in lakes with contrasting extremes of reflectance, *Limnol. Oceanogr.*, *53*, 2021–2034, doi:10.4319/lo.2008.53.5.2021.

Gordon, H. R., O. B. Brown, and M. M. Jacobs (1975), Computed relationships between the inherent and apparent optical properties of a flat homogeneous ocean, *Appl. Opt.*, *14*, 417–427, doi:10.1364/AO.14.000417.

Harding, L. W. J. (1994), Long-term trends in the distribution of phytoplankton in Chesapeake Bay: Roles of light, nutrients and streamflow, *Mar. Ecol. Prog. Ser.*, *104*, 267–291, doi:10.3354/meps104267.

Hirata, T., and N. K. Højerslev (2008), Relationship between the irradiance reflectance and inherent optical properties of seawater, *J. Geophys. Res.*, *113*, C03030, doi:10.1029/2007JC004325.

Huot, Y., A. Morel, M. S. Twardowski, D. Stramski, and R. A. Reynolds (2008), Particle optical backscattering along a chlorophyll gradient in the upper layer of the eastern South Pacific Ocean, *Biogeosciences*, *5*, 495–507, doi:10.5194/bg-5-495-2008.

Idso, S. B., and R. G. Gilbert (1974), On the universality of the Poole and Atkins Secchi disk-light extinction equation, *J. Appl. Ecol.*, *11*, 399–401, doi:10.2307/2402029.

Jassby, A. D., J. E. Reuter, and C. R. Goldman (2003), Determining long-term water quality change in the presence of climate variability: Lake Tahoe (U.S.A.), *Can. J. Fish. Aquat. Sci.*, *60*, 1452–1461, doi:10.1139/f03-127.

Kemp, W. M., et al. (2004), Habitat requirements for submerged aquatic vegetation in Chesapeake Bay: Water quality, light regime, and physical-chemical factors, *Estuaries*, *27*, 363–377, doi:10.1007/BF02803529.

Kirk, J. T. O. (1981), Monte Carlo study of the nature of the underwater light field in, and the relationships between optical properties of, turbid, yellow waters, *Aust. J. Mar. Freshwater Res.*, *32*, 517–532, doi:10.1071/MF9810517.

Kirk, J. T. O. (1984), Dependence of relationship between apparent and inherent optical properties of water on solar altitude, *Limnol. Oceanogr.*, *29*, 350–356, doi:10.4319/lo.1984.29.2.0350.

Kirk, J. T. O. (1994), The relationship between the inherent and the apparent optical properties of surface waters and its dependence on the shape of the volume scattering function, in *Ocean Optics*, edited by R. W. Spinrad, K. L. Carder, and M. J. Perry, pp. 40–58, Oxford Univ. Press, Oxford, U. K.

Koenings, J. P., and J. A. Edmundson (1991), Secchi disk and photometer estimates of light regimes in Alaskan lakes: Effects of yellow color and turbidity, *Limnol. Oceanogr.*, *36*, 91–105, doi:10.4319/lo.1991.36.1.0091.

Lee, Z.-P., K. L. Carder, S. K. Hawes, R. G. Steward, T. G. Peacock, and C. O. Davis (1994), Model for the interpretation of hyperspectral remote-sensing reflectance, *Appl. Opt.*, *33*, 5721–5732, doi:10.1364/AO.33.005721.

Lee, Z.-P., K. P. Du, and R. Arnone (2005), A model for the diffuse attenuation coefficient of downwelling irradiance, *J. Geophys. Res.*, *110*, C02016, doi:10.1029/2004JC002275.

Lewis, M. R., R. E. Warnock, and T. Platt (1985), Absorption and photosynthetic action spectra for natural phytoplankton populations: Implications for production in the open ocean, *Limnol. Oceanogr.*, *30*, 794–806, doi:10.4319/lo.1985.30.4.0794.

Loisel, H., X. Mériaux, J.-F. Berthon, and A. Poteau (2007), Investigation of the optical backscattering to scattering ratio of marine particles in relation to their biogeochemical composition in the eastern English Channel and southern North Sea, *Limnol. Oceanogr.*, *52*, 739–752, doi:10.4319/lo.2007.52.2.0739.

Magnuson, A., L. W. Harding Jr., M. E. Mallonee, and J. E. Adolf (2004), Bio-optical model for Chesapeake Bay and the Middle Atlantic Bight, *Estuarine Coastal Shelf Sci.*, *61*, 403–424, doi:10.1016/j.ecss.2004.06.020.

McClelland, J. W., and I. Valiela (1998), Changes in food web structure under the influence of increased anthropogenic nitrogen inputs to estuaries, *Mar. Ecol. Prog. Ser.*, *168*, 259–271, doi:10.3354/meps168259.

Mobley, C. D. (1994), *Light and Water: Radiative Transfer in Natural Waters*, Academic, San Diego, Calif.

Mobley, C. D., and D. Stramski (1997), Effects of microbial particles on oceanic optics: Methodology for radiative transfer modeling and example simulations, *Limnol. Oceanogr.*, *42*, 550–560, doi:10.4319/lo.1997.42.3.0550.

Morel, A., and Y.-H. Ahn (1990), Optical efficiency factors of free-living marine bacteria: Influence of bacterioplankton upon the optical properties and particulate organic carbon in oceanic waters, *J. Mar. Res.*, *48*, 145–175, doi:10.1357/002224090784984632.

Morel, A., and Y.-H. Ahn (1991), Optics of heterotrophic nanoflagellates and ciliates: A tentative assessment of their scattering role in oceanic waters compared to those of bacterial and algal cells, *J. Mar. Res.*, *49*, 177–202, doi:10.1357/002224091784968639.

Morel, A., and B. Gentili (1993), Diffuse reflectance of oceanic waters. II. Bidirectional aspects, *Appl. Opt.*, *32*, 6864–6879, doi:10.1364/AO.32.006864.

Morel, A., D. Antoine, and B. Gentili (2002), Bidirectional reflectance of oceanic waters: Accounting for Raman emission and varying particle scattering phase function, *Appl. Opt.*, *41*, 6289–6306, doi:10.1364/AO.41.006289.

Passow, U. (2002), Transparent exopolymer particles (TEP) in aquatic environments, *Prog. Oceanogr.*, *55*, 287–333, doi:10.1016/S0079-6611(02)00138-6.

Pegau, W. S., D. Gray, and J. R. V. Zaneveld (1997), Absorption and attenuation of visible and near-infrared light in water: Dependence on temperature and salinity, *Appl. Opt.*, *36*, 6035–6046, doi:10.1364/AO.36.006035.

Peng, F., and S. W. Effler (2007), Suspended minerogenic particles in a reservoir: Light-scattering features from individual particle analysis, *Limnol. Oceanogr.*, *52*, 204–216, doi:10.4319/lo.2007.52.1.0204.

Petzold, T. J. (1972), Volume scattering functions for selected ocean waters, *Tech. Rep., SIO Ref. 72–78*, 79 pp., Visibility Lab., Scripps Inst. of Oceanogr., San Diego, Calif.

Platt, T., and A. W. Herman (1983), Remote sensing of phytoplankton in the sea: Surface-layer chlorophyll as an estimate of water-column chlorophyll and primary production, *Int. J. Remote Sens.*, *4*, 343–351, doi:10.1080/01431168308948552.

Platt, T., and S. Sathyendranath (1988), Oceanic primary production: Estimation by remote sensing at local and regional scales, *Science*, *241*, 1613–1620, doi:10.1126/science.241.4873.1613.

Platt, T., S. Sathyendranath, and P. Ravindran (1990), Primary production by phytoplankton: Analytic solutions for daily rates per unit area of water surface, *Proc. R. Soc. London, Ser. B*, *241*, 101–111, doi:10.1098/rspb.1990.0072.

Poole, H. H., and W. R. G. Atkins (1929), Photo-electric measurements of submarine illumination throughout the year, *J. Mar. Biol. Assoc. U. K.*, *16*, 297–324, doi:10.1017/S0025315400029829.

Pope, R. M., and E. S. Fry (1997), Absorption spectrum (380–700) nm of pure water. II. Integrating cavity measurements, *Appl. Opt.*, *36*, 8710–8723, doi:10.1364/AO.36.008710.

Preisendorfer, R. W. (1961), Application of radiative transfer theory to light measurement in the sea, *Int. Union Geod. Geophys. Monogr.*, *10*, 11–30.

Preisendorfer, R. W. (1986), Secchi disk science: Visual optics of natural waters, *Limnol. Oceanogr.*, *31*, 909–926, doi:10.4319/lo.1986.31.5.0909.

Preston, B. L. (2004), Observed winter warming of the Chesapeake Bay estuary (1949–2002), Implications for ecosystem management, *Environ. Manage. N. Y.*, *34*, 125–139, doi:10.1007/s00267-004-0159-x.

Ryther, J. H., and C. S. Yentsch (1957), The estimation of phytoplankton production in the ocean from chlorophyll and light data, *Limnol. Oceanogr.*, *2*, 281–286.

Snyder, W. A., et al. (2008), Optical scattering and backscattering by organic and inorganic particulates in U.S. coastal waters, *Appl. Opt.*, *47*, 666–677, doi:10.1364/AO.47.000666.

Stramski, D., A. Bricaud, and A. Morel (2001), Modeling the inherent optical properties of the ocean based on the detailed composition of the planktonic community, *Appl. Opt.*, *40*, 2929–2945, doi:10.1364/AO.40.002929.

Stramski, D., E. Boss, D. Bogucki, and K. J. Voss (2004), The role of seawater constituents in light backscattering in the ocean, *Prog. Oceanogr.*, *61*, 27–56, doi:10.1016/j.pocean.2004.07.001.

Swift, T. J., J. Perez-Losada, S. G. Schladow, J. E. Reuter, A. D. Jassby, and C. R. Goldman (2006), Water clarity modeling in Lake Tahoe: Linking suspended matter characteristics to Secchi depth, *Aquat. Sci.*, *68*, 1–15, doi:10.1007/s00027-005-0798-x.

Tassan, S., and G. M. Ferrari (2003), Variability of light absorption by aquatic particles in the near-infrared spectral region, *Appl. Opt.*, *42*, 4802–4810, doi:10.1364/AO.42.004802.

Twardowski, M. S., E. Boss, J. B. Macdonald, W. S. Pegau, A. H. Barnard, and J. R. V. Zaneveld (2001), A model for estimating bulk refractive index from the optical backscattering ratio and the implications for understanding particle composition in case I and case II waters, *J. Geophys. Res.*, *106*, 14,129–14,142, doi:10.1029/2000JC000404.

Tyler, J. E. (1968), The Secchi disc, *Limnol. Oceanogr.*, *13*, 1–6, doi:10.4319/lo.1968.13.1.0001.

Tzortziou, M., J. R. Herman, C. L. Gallegos, P. J. Neale, A. Subramaniam, L. W. Harding Jr., and Z. Ahmad (2006), Bio-optics of the Chesapeake

Bay from measurements and radiative transfer closure, *Estuarine Coastal Shelf Sci.*, *68*, 348–362, doi:10.1016/j.ecss.2006.02.016.

Werdell, P. J., S. W. Bailey, B. A. Franz, L. W. Harding Jr., G. C. Feldman, and C. R. McClain (2009), Regional and seasonal variability of chlorophyll-a in Chesapeake Bay as observed by SeaWiFS and MODIS-Aqua, *Remote Sens. Environ.*, *113*, 1319–1330, doi:10.1016/j.rse.2009.02.012.

Wetz, M., M. Robbins, and H. Paerl (2009), Transparent exopolymer particles (TEP) in a river-dominated estuary: Spatial-temporal distributions and an assessment of controls upon TEP formation, *Estuaries Coasts*, *32*, 447–455, doi:10.1007/s12237-009-9143-2.

Woźniak, B., and J. Dera (2007), *Light Absorption in Sea Water*, Springer, New York.

Woźniak, S. B., and D. Stramski (2004), Modeling the optical properties of mineral particles suspended in seawater and their influence on ocean reflectance and chlorophyll estimation from remote sensing algorithms, *Appl. Opt.*, *43*, 3489–3503, doi:10.1364/AO.43.003489.

Woźniak, S. B., D. Stramski, M. Stramska, R. A. Reynolds, V. M. Wright, E. Y. Miksic, M. Cichocka, and A. M. Cieplak (2010), Optical variability of seawater in relation to particle concentration, composition, and size distribution in the nearshore marine environment at Imperial Beach, California, *J. Geophys. Res.*, *115*, C08027, doi:10.1029/2009JC005554.

Zervas, C. (2009), Sea level variations of the United States 1854–2006, *Tech. Rep., NOS CO-OPS 053*, 176 pp., NOAA, Washington, D. C.

C. L. Gallegos, Smithsonian Environmental Research Center, PO Box 28, Edgewater, MD 21037, USA. (gallegosc@si.edu)

C. R. McClain and P. J. Werdell, Ocean Ecology Branch, NASA Goddard Space Flight Center, Code 614.2, Greenbelt, MD 20771, USA.